Swiss Journal of Geosciences

Performance of the Opalinus Clay under thermal loading. Experimental results from Mont Terri rock laboratory (Switzerland)

--Manuscript Draft--

Manuscript Number:	SJGS-D-16-00043R4
Full Title:	Performance of the Opalinus Clay under thermal loading. Experimental results from Mont Terri rock laboratory (Switzerland)
Article Type:	Original Paper
Corresponding Author:	Antonio Gens, Ph.D. Universitat Politecnica de Catalunya SPAIN
Corresponding Author Secondary Information:	
Corresponding Author's Institution:	Universitat Politecnica de Catalunya
Corresponding Author's Secondary Institution:	
First Author:	Antonio Gens, Ph.D.
First Author Secondary Information:	
Order of Authors:	Antonio Gens, Ph.D.
	Klaus Wieczorek
	Irina Gaus
	Benoit Garitte
	Juan Carlos Mayor
	Kristof Schuster
	Gilles Armand
	Jose Luis Garcia Siñeriz
	Thomas Trick
Order of Authors Secondary Information:	
Funding Information:	
Abstract:	The paper presents an overview of the behaviour of Opalinus Clay under thermal loading as observed in three in-situ heating tests performed in the Mont Terri rock laboratory: HE-B, HE-D and HE-E. The three tests are summarily described; they encompass a broad range of test layouts and experimental conditions. Afterwards, the following topics are examined: determination of thermal conductivity, thermally-induced pore pressure generation and thermally-induced mechanical effects. The mechanisms underlying pore pressure generation and dissipation are discussed in detail and the relationship between rock damage and thermal loading is examined using an additional in-situ test: SE-H. The paper concludes with an evaluation of the various thermo-hydro-mechanical (THM) interactions identified in the heating tests.
Response to Reviewers:	

Performance of the Opalinus Clay under thermal loading. Experimental results from Mont Terri rock laboratory (Switzerland)

Antonio Gens*[1)], Klaus Wieczorek[2)], Irina Gaus[3)], Benoit Garitte[3)], Juan Carlos Mayor[4)], Kristof Schuster[5)], Gilles Armand[6)], José Luis García-Siñeriz[7)] and Thomas Trick[8)]

1) Universitat Politècnia de Catalunya, Jordi Girona 1-3, 08034 Barcelona, Spain
2) GRS, Theodor-Heuss-Straße 4, 38122 Braunschweig, Germany
3) Nagra, Hardstrasse 73, 5430 Wettingen, Switzerland
4) Enresa, Emilio Vargas 7, 28043 Madrid, Spain
5) BGR, Stilleweg 2, 30655 Hannover, Germany
6) Andra, 1 Rue Jean Monnet, 92290 Châtenay-Malabry, France
7) AITEMIN, Margarita Salas 14, 28918 Leganés (Madrid), Spain
8) Solexperts, Mettlenbachstrasse 25, 8617 Mönchaltorf, Switzerland

Corresponding author: Antonio Gens. E-mail: antonio.gens@upc.edu

Running title: Performance of the Opalinus Clay under thermal loading

Keywords: temperature effects, in-situ tests, coupled THM phenomena, numerical analyses, heating tests, pore pressures

Abstract

The paper presents an overview of the behaviour of Opalinus Clay under thermal loading as observed in three in-situ heating tests performed in the Mont Terri rock laboratory: HE-B, HE-D and HE-E. The three tests are summarily described; they encompass a broad range of test layouts and experimental conditions. Afterwards, the following topics are examined: determination of thermal conductivity, thermally-induced pore pressure generation and thermally-induced mechanical effects. The mechanisms underlying pore pressure generation and dissipation are discussed in detail and the relationship between rock damage and thermal loading is examined using an additional in-situ test: SE-H. The paper concludes with an evaluation of the various thermo-hydro-mechanical (THM) interactions identified in the heating tests.

1 Introduction

Opalinus Clay has been selected in Switzerland as the preferred host rock for disposal of high-level nuclear waste. In this context, the behaviour of Opalinus Clay is being intensively investigated in the Mont Terri rock laboratory, an international project that has been ongoing since 1996. Figure 1 shows the geological profile of the site. The exothermic nature of high-level radioactive waste requires studies that target the performance of Opalinus Clay under non-isothermal conditions so that the impact of heat on the geological barrier becomes well understood.

The behaviour of an indurated mudstone, such as Opalinus Clay, under thermal loading has to be considered in the framework of thermo-hydro-mechanical (THM) couplings as the various THM phenomena interact. Thus, temperature variations will impact hydraulic behaviour due to the generation of pore pressures and the variation of fluid viscosity and will affect the

mechanical behaviour through the development of thermally-induced strains. Hydraulic and mechanical behaviour may interact with the thermal response through induced variations of thermal conductivity. Heat convection is also a potential effects of hydraulic behaviour on the temperature field although it is generally negligible in a low permeability medium. Figure 2 shows a scheme indicating the relationship between the most relevant thermal, hydraulic and mechanical phenomena where the hydromechanical interactions have also been included. As discussed later, not all the interactions have the same level of significance.

To examine the thermal behaviour of Opalinus Clay as well the associated coupled THM effects, a number of thermal in-situ tests have been performed in the Mont Terri rock laboratory: HE-B (initially called HE), HE-C, HE-D, HE-S, SE-H, HE-E and FE. Some of them, such as HE-E and FE, are still ongoing. There have also been projects involving only small-scale tests such as LT (Laboratory temperature testing) and TH-A (microscale THMC). More details are given in Wileveau et al (2008).

This paper focuses on the behaviour of Opalinus Clay under thermal loading as observed in three main heating field tests: HE-B, HE-D and HE-E that are summarily described first. Afterwards, the results of those in-situ tests are reviewed in order to examine more closely the behaviour of Opalinus Clay under thermal loading. Specifically, the following aspects are discussed: thermal conductivity, pore pressure generation (thermo-hydraulic coupling) and mechanical effects such as strain development and thermally-induced damage. The paper concludes with a discussion on the coupled THM phenomena as observed in Opalinus Clay

2 The main in-situ heating tests

The three Mont Terri rock laboratory in-situ heating tests considered are: HE-B, HE-D and HE-E. They encompass a variety of features concerning the geometrical setting, presence and type of backfill, maximum temperature and heating duration. Table 1 contains the main characteristics of the tests whereas Figure 3 shows their location in the Mont Terri rock laboratory. At the Mont Terri rock laboratory, the overburden height varies between 250 m and 320 m. Opalinus Clay is intensively bedded; the closely-spaced bedding planes dip at an angle of approximately 45º at the laboratory location. All tests have been performed in the shaly facies of Opalinus Clay.

2.1 The HE-B experiment

The HE-B experiment involved placing a heater of 0.1 m diameter and 2.02 m long in a 300mm diameter vertical borehole. The borehole was 7.5m deep and was drilled in a niche excavated for this purpose. The heater was surrounded by a compacted clay barrier made up of ring-shaped Febex bentonite blocks with a dry density of 1.8 g/cm^3. 19 boreholes were drilled in the niche floor to install sensors to measure temperature, relative humidity, total stresses, pore pressures, displacements and electrical resistivity. Devices to determine gas and water release were also installed in the boreholes. The layout of the main borehole containing the heater and the distribution of the monitoring boreholes in the niche are depicted in Figure 4.

Before heating was started, the barrier was hydrated artificially for 35 months using synthetic Pearson water (similar in chemical composition to the water present in the Opalinus Clay). Afterwards heating was applied during a 18th month period. Once a maximum temperature of

100ºC was reached in the bentonite, heater power was adjusted in order to keep that maximum temperature constant. The heating period of the experiment spanned from February 2002 to the end of August 2003. At the end of the heating period, the heater was switched off and, after 1 month cooling period, the test was dismantled. Geotechnical, hydraulic and seismic field tests were performed at the end of the test and a number of rock samples were retrieved for testing in the laboratory. A full description of the test has been presented in Göbel et al. (2007), only some representative results are shown here.

Figure 5 shows the distribution of temperatures of the rock (at the central section of the heater) at different times of the heating test. It can be observed that, although a 100ºC temperature was applied by the heater, the maximum rock temperature only reached about 40ºC and dropped rapidly with distance. This is the consequence of the layout of the test (a single heater borehole) and the insulating nature of the bentonite barrier. In spite of the modest increase in temperature, significant pore pressures develop in the Opalinus Clay (Fig. 6). A fast initial development of pore pressures followed by a more gradual dissipation can be observed. The final sudden pore pressure drop is due to the cooling period that followed the switching off of the heater. Higher temperatures in borehole BHE-19 (located at 0.65, from the central borehole axis) give rise to higher pore pressures than those measured in borehole BHE-20 located 2 meters away and subjected, therefore, to lower temperatures.

2.2 The HE-D experiment

To perform the in-situ heating test HE-D a niche was also excavated off Gallery 98 from which a 30 cm diameter borehole (D0) was drilled horizontally up to a total length of 14 m. A location was selected away from previous experiments in order to test intact rock properties.

In the section close to the end of the borehole, two heaters were installed. The heaters were 2m long and their separation was 0.8m, In this case there was no bentonite barrier and the heaters were in direct contact with Opalinus Clay. To achieve a good contact with the rock, the heaters were pressurized to 1 MPa. In addition, a number of auxiliary boreholes have been constructed to install a variety of instruments for monitoring the test. Figure 7 shows a top view of the test area. A horizontal test layout was chosen in order to have a largely uniform lithology.

Temperatures were measured along two boreholes drilled (D1 and D2) from the niche HE-D. However, perhaps the most relevant observations were those combining measurements of temperatures and pore pressures at the same point in order to relate directly the two variables. This was achieved in borehole D3 (drilled parallel to the heater borehole) and in a series of small diameter boreholes (D7 to D17) drilled from the MI niche. The pore pressure measurements of sensors located below the main borehole were quite successful but the pore pressure probes located above the main borehole exhibited a rather slow response attributed to difficulties encountered in de-airing the sensor area. Finally, sliding micrometer tubing was installed in boreholes D4 and D5 to measure incremental deformations at 1 m intervals. Special care was taken to ensure accuracy in the direction and length of the instrumentation boreholes to guarantee the correct location of the sensors. All instruments were in place before the drilling of the main borehole containing the heaters. In this way hydro-mechanical effects during excavation could also be recorded. Full information on the test is given in Wileveau (2005).

Approximately one month after installation and pressurization, the heaters were switched on with a total power of 650 W (325 W per heater). The heaters were then left under constant

power during 90 days. Afterwards the power was increased threefold, to 1950 W (975W per heater) and maintained at that level for 248 days more. The heating period lasted form March 2004 to February 2005. At the end of the second heating stage, the heaters were switched off and the clay was allowed to cool down. Temperatures, pore pressures and deformations were measured throughout. Examples of the observations obtained are shown in Figures 8 and 9 in terms of evolution of temperatures and pore pressures at different distances from the heaters. The pattern of results is similar to that of the HE-B experiment but the increase of pore pressure is now significantly higher as a result of the different test design.

2.3 The HE-E experiment

The HE-E experiment has been installed in a section of the 1.3 m diameter and 50 m long microtunnel excavated in 1999 using the raised-boring technique. The same section of the microtunnel had been used previously for a ventilation test (VE). The layout of the experiment is shown in Figure 10. Two 4 m-long heaters have been used separated by a plug. Heater 1 is surrounded by an engineer barrier composed of granular MX-80 bentonite made up of pellets with a mean diameter 1 mm approximately and sits on a bed of MX-80 compacted blocks. The dry bulk density of the granular bentonite as placed is 1.46 g/cm^3 and the dry density of the blocks is 1,806 g/cm^3. The arrangement of Heater 2 is the same except that the granular material used in the barrier is a mixture of sand and MX-80 bentonite. The resulting dry density of the granular sand/pellet mixture is 1.50 g/cm^3. No artificial hydration is used for saturating the engineered barrier, so water uptake by the bentonite will be very limited due to the low permeability of the Opalinus Clay.

Extensive instrumentation was used to monitor the progress of the test in the following locations: i) the heater surface where the temperature is controlled, ii) the engineered barrier and the interface with the Opalinus Clay (temperature and relative humidity), iii) the Opalinus Clay close to the microtunnel using the sensors from the VE test (temperature, humidity, water pressure and displacement), and iv) the Opalinus Clay at distances ranging from 2 to 6 meters from the microtunnel (pore pressures). This test is fully described in Gaus et al. (2014).

The heating stage started at the end of June 2011 and it is still ongoing at present as this experiment is intended as a long-term test. Heating power was gradually raised over a period of one year approximately until reaching a maximum temperature on the heater surfaces of 140ºC. From that moment on, heater power has been adjusted to keep this control temperature constant. Figure 11 shows the recorded evolution of heater power. The observed difference between the two heaters is due to the different thermal conductivities of the two materials used for the engineered barriers. The evolution of the temperatures in Opalinus Clay close to heater 1 is presented in Figure 12. It can be seen that close to the tunnel/barrier interface the temperature has reached 90 ºC but it drops sharply as the distance to the tunnel increases.

Figure 13 shows the evolution of thermally-induced pore pressures at distances ranging from 3.5 to 5.5 meters. It can be observed that at the end of the period considered, pore pressure reduction is not apparent yet.

.

The HE-E test has a number of novel features such as a temperature higher than 100ºC, natural hydration and granular bentonite used in the engineered barrier, enlarging in this way the range of conditions under which the response of Opalinus Clay has been observed. In spite of the differences between the three tests, the basic characteristics of the response are quite similar so that they can be used to derive some general observations on the non-isothermal

behaviour of Opalinus Clay, as described in the following sections. The main effort is placed in the analysis of the HE-D test as it is not affected by the presence of an engineered barrier and the behaviour of the Opalinus Clay can be observed in a more direct manner.

.

3 Thermal conductivity

The low permeability of Opalinus Clay ensures that the heat transport by advection is negligible; conduction is the only relevant heat transfer mechanism. Therefore, the thermal field is basically controlled by the value of thermal conductivity, λ, the coefficient that links, in Fourier's law, the conductive flux, $\mathbf{i}_c$, to the gradient of temperature, T:

$$\mathbf{i}_c = \lambda \nabla T \tag{1}$$

Although tests HE-B and HE-E have been analysed assuming an isotropic thermal conductivity (Göbel et al 2007; Gaus et al. 2014), it is well established that thermal conductivity of Opalinus Clay is anisotropic (Bossart 2008) exhibiting different values in the directions normal and parallel to bedding. With the coordinates aligned adequately, equation (1) becomes:

$$\mathbf{i}_c = \begin{bmatrix} \lambda_{par} & 0 & 0 \\ 0 & \lambda_{par} & 0 \\ 0 & 0 & \lambda_{per} \end{bmatrix} \cdot \nabla T \tag{2}$$

where λ_{par} and λ_{per} are the thermal conductivity values in the bedding plane and in the perpendicular direction, respectively.

If a sufficient number of temperature measurements are available, it is in principle possible to estimate the thermal conductivity values form a backanalysis of an in-situ heating test. Because the thermal problem is largely independent of the hydromechanical one, performing

a purely thermal analysis suffices. However, as demonstrated by Garitte et al. (2014), there are pitfalls if a conventional backanalysis is performed in which a least square criterion is applied blindly to the ensemble of all the results giving the same weight to all of them. Such conventional analysis can easily provide biased results depending on the sequence of observation times considered as well as on the location of the sensors.

In this context, the analysis of a synthetic case consisting of a heat point source has provided key insights. This problem has an analytical solution (Booker and Savidou 1985) that can be applied to anisotropic thermal conductivity conditions using an equivalent thermal conductivity (Carslaw and Jaeger 1946):

$$\lambda_0 = \sqrt[3]{\lambda_{par} \cdot \lambda_{par} \cdot \lambda_{per}} \tag{3}$$

Figure 14 shows the thermal conductivity parameter pairs that provide a good agreement (i.e. an error of less than 2%) with the analytical solution. It can be noted that the combination of the thermal parameters vary depending on the time at which the backanalysis is performed. The Figure clearly indicates that short term and long term observations provide different information on the combinations of λ_{par} and λ_{per} that provide a good representation of the results. Therefore, to identify independently the two thermal conductivity values, it is essential to combine the short term and the long term observations in an appropriate manner. Building on those observations, the following procedure was recommended (Garitte et al. 2014):

i) 3D analyses of the experiment considered are performed using different thermal conductivity pairs covering a wide range. 3D analyses are required to take into account anisotropy.

ii) Values of thermal conductivity minimizing the difference between observations and calculations are obtained for each individual sensor and for each heating phase. The determination of the pair of thermal conductivity values is performed from the combination of short term and long term data. Outliers are removed from the backanalysis.

iii) An overall value of thermal conductivities is obtained from the average of all the sensors. If there are significantly different numbers of sensors aligned parallel and perpendicular to the bedding planes, the average of each orientation will be computed first and a final overall value will be obtained from the average of the sensors at the two different orientations.

The analyses for the synthetic case also allowed identifying the effects of experimental uncertainties in sensor location, power input, temperature measurements and specific heat. For instance, if there is a significant difference between the thermal conductivities computed from sensors parallel and perpendicular to bedding planes, it is an indication of uncertainty in the heating power that may then be adjusted accordingly.

The procedure just outlined has been applied to the observations of the HE-D test. The results are shown in Figure 15 (Garitte et al. 2014). It can be noted that the parallel sensors and the perpendicular sensors tend to indicate different thermal conductivity pairs. Some power loss was assumed as a possible explanation for this kind of pattern and a second analysis was accordingly performed. Diamond dots indicate the analysis in which no power loss was applied and circle dots indicate the best-fitting thermal conductivity pairs determined in an analysis considering a power loss of 5%. Due to the differences between the two sensor groups and to the fact that more perpendicular sensors were available in the HE-D experiment, the averages of the perpendicular sensors and of the parallel sensors are done first and then

the final average is computed. In this way, the best estimates for the thermal conductivity are: λ_{par}= 2.15 W/mºK and λ_{per}= 1.2 W/mºK, an anisotropy ratio of 1.8. Those values are remarkably close to those obtained in the laboratory (Bossart 2008). It is also interesting that the backcalculated values for all sensors tend to cluster close to a value of equivalent thermal conductivity of about 1.8 W/mºK.

4. Thermally-induced pore pressure generation

In Opalinus Clay, the main hydraulic phenomenon associated with thermal effects is the generation of pore pressure due to changes of temperature. When Opalinus Clay (and other argillaceous rocks) is subjected to a temperature increase, the pore pressure will also increase due to the fact that the thermal expansion of the water is larger than that of the porous skeleton itself. The low permeability of Opalinus Clay ensures that the resulting excess pore pressure does not dissipate rapidly. As a matter of fact, quite a number of interactions underlie this pore pressure generation phenomenon; they are best viewed by considering the water mass balance equation:

$$n\frac{D_s\rho_w}{Dt}+\frac{\rho_w}{\rho_s}\cdot(1-n)\cdot\frac{D_s\rho_s}{Dt}+\rho_w\cdot\nabla\cdot\frac{d\mathbf{u}}{dt}+\nabla\cdot(\rho_w\cdot q_l)=0 \tag{4}$$

where n is the porosity, ρ_w and ρ_s are the water and solid densities respectively, t is time, **u** are displacements and q_l is Darcy's liquid velocity. D_s denotes material derivative.

Equation (4) can be further developed taking into account the variation of the liquid and solid densities that, with some simplifications, are assumed to be given by:

$$\rho_w=\rho_{w0}\cdot\exp\left[\beta_w(p_l-p_{lo})+b_w(T-T_{ref})\right] \tag{5}$$

$$\rho_s=\rho_{s0}\cdot\exp\left[\beta_s(p_s-p_{so})+3\cdot b_s\cdot\left(T-T_{ref}\right)\right] \tag{6}$$

where β_w and β_s are the water and solid compressibilities, respectively, and b_w and b_s are the volumetric and linear thermal expansion coefficient for water and the solid phase, respectively. p_l is the liquid pressure, p_s is the solid pressure, and T is temperature.

Then equation (4) becomes:

$$\left[n \cdot b_w + (1-n) \cdot 3 \cdot b_s\right] \cdot \frac{D_s T}{Dt} + n \cdot \beta_w \cdot \frac{D_s p_l}{Dt} + (1-n) \cdot \beta_s \cdot \frac{D_s p_s}{Dt} + \nabla \cdot \frac{d\mathbf{u}}{dt} + \frac{\nabla \cdot (\rho_w \cdot q_l)}{\rho_w} = 0 \qquad (7)$$

The generation and dissipation of pore pressure in the clay due to a temperature change can be more readily understood examining equation (7). The first term arises from the differential thermal expansion of solid and liquid phases. The second and third terms are the volume changes of water and solid phase associated with a pore pressure and solid pressure change; the fourth term is the volume change of the material skeleton (that includes contributions from stresses, pore pressures and temperature) and the fifth term corresponds to the flow of water in or out of the clay element considered. The interplay of all those phenomena results in the generation of pore pressure and its evolution with time.

Interesting insights can be obtained examining a typical evolution of temperature and pore pressure as presented in Figure 16. It was recorded in borehole D3 (Fig. 7) with the sensors located 1.1 m away from the axis of the heater in the direction of the bedding planes. It can be observed that pore pressures react immediately to heating, exhibiting a very strong response. Increments of 2.25 MPa are measured at this particular location; this is a magnitude similar to the estimated minor principal stress in the area. It is also interesting to note that the evolutions of temperature and pore pressures do not coincide. Pore pressure reaches a maximum at a particular time and then it decreases in spite of the fact that temperature continues to rise. This is the result of the interplay between the generation of pore pressures due to thermal action

and the dissipation of pore pressures due to consolidation. At this particular location, dissipation by liquid-flow overcomes the temperature increase effects in the later stages of the experiment.

A numerical three-dimensional coupled THM analysis was performed so that the anisotropy of the material (thermal conductivity and stiffness) and of the in-situ stress system could be incorporated in the calculations. Due to the special characteristics of Opalinus Clay, a constitutive model that tries to account for the fact that the microstructure of the material is a combination of clay matrix and cementing bonds have been used (Vaunat and Gens 2003a, 2003b). A full description of the numerical modelling of the in-situ test as well as the parameters used is presented in Gens et al. (2007).

Figure 17 presents, for a number of points of the clay, the comparison between the results of the 3D analysis and the observations in terms of pore pressure increases. The results of two companion axisymmetric analyses have also been added for reference. The maximum pore pressure increase is largely well captured and the evolution of pore pressure is also well reproduced with the exception of borehole D17 located further away from the heaters. The pore pressure rise obtained in the computations in the first heating stage is faster than the observed one. This could be due to a slow response of the pore pressure sensors; it can be noted that in the second stage, when the piezometers are likely to be fully saturated, the observed and computed rate of pore pressure increase appear to be the same.

In Figure 17, it can also be noted that the time at which the maximum pore pressure increase is calculated becomes larger as the distance to the main borehole increases. This is a consequence of the combined effect of the movement of the temperature rise outwards and of

pore pressure dissipation from the inner zones. Computed pore pressure distributions on a section perpendicular to the main borehole and located between the two heaters are plotted for various times in Figure 18. They correspond to two perpendicular directions; one along the bedding plane direction and the other one along a direction normal to the bedding. The differences that can be observed between the distributions in the two directions are not caused by hydraulic effects (permeability was assumed isotropic) but they arise from the different temperature rise brought about by the anisotropy of thermal conductivity.

The anisotropy and the evolution of pore pressures can also be observed in the contours of equal pore pressure presented in Figure 19 where the displacement with time of the maximum of pore pressure away from the main borehole can be observed. The Figure also shows that the cooling associated with the switching off of the heaters produces a reduction in pore pressure, the counterpart of the pore pressure rise during heating.

Availability of a successfully validated numerical model allows the performance of a series of sensitivity analyses to explore the potential effects of a number of parameters and, in this way, improve the understanding of the mechanisms causing the thermally-induced generation of pore-water pressures. The values of Young's modulus, Biot coefficient, solid compressibility, thermal expansion coefficients and thermal conductivity have been varied over a rather wide range. In all cases, the effect on the generated pore pressures was found to be either modest or negligible (Gens et al. 2007).

The effect of intrinsic water permeability is however very significant. This is not surprising because the magnitude of the pore pressure generated results from a competition between the effects of differential thermal expansion of liquid and clay skeleton and the dissipation of pore

pressures, the rate of which is controlled basically by the value of rock permeability. The results of sensitivity analyses with values of intrinsic permeability varying in the plausible range (for Opalinus Clay) of 10^{-19} m^2 to 10^{-20} m^2 (the reference value is 5×10^{-20} m^2) are shown in Figure 20a. The effect on generated pore pressures is large. Because of the weight of this parameter in the global behaviour of the test, two additional analyses have been performed using intrinsic permeabilities of 10^{-23} m^2 and 10^{-16} m^2 to correspond to practically undrained and practically drained conditions. As Figure 20b shows, in the very low permeability case there is an extremely large increase of pore pressures that tracks closely the temperature evolution; dissipation is practically negligible and undrained conditions predominate. In contrast, Figure 20b also shows that in the very large permeability case no pore pressure generation is observed since pore pressure dissipation dominates throughout. It should be noted that although Opalinus Clay is a low permeability material, pore pressure dissipation plays a critical role with respect to the magnitude of the pore pressures generated by thermal action. If there were no dissipation, pore pressures would reach values above 12 MPa in the rock close to the heater.

5. Thermally-induced mechanical effects

Mechanical effects result from the joint action of temperature changes and pore pressure generation and dissipation. They can be perceived from the measurements of relative displacements in boreholes D4 and D5 performed using a sliding micrometer (Fig. 7). Borehole D5 was drilled at a direction approximately normal to the main borehole containing the heaters; the deformations measured at various times are plotted in Figure 21. It can be observed that in the region around the heaters, extension deformations occur, but they become compressive strains at locations further away from the heater. The volume increase of the clay close to the heater, driven by thermal expansion, produces compression in the outer zones.The

evolution of strains of some selected intervals of borehole D5 is shown in Figure 22 together with the computed results from the analyses. A thermal expansion coefficient of 1.4×10^{-5} K^{-1} has been adopted, following Auvray (2004). A first observation is the very small magnitude of the strains (and hence displacements) measured and computed, consistent with the high stiffness and modest thermal expansion exhibited by Opalinus Clay.

In borehole intervals close to the heater (e.g. intervals 6-7, 7-8 and 8-9 of borehole D-5) dilatant strains are observed in response of the temperature increase; the two heating stages can be easily recognized. In contrast, in borehole intervals away from the heater (e.g. intervals 11-12 and 12-13), compressive strains are measured in the initial stages due to the expansion of the inner regions of the test. As the temperature increase field spreads out with time, the rock expands and dilatant strains are observed and computed. In spite of some scatter of the observations (due to the small magnitudes being measured), the numerical analyses capture satisfactorily the main patterns of behaviour.

Unfortunately no direct observations of damage in terms of permeability variations were obtained in test HE-D. So, the potential effect of heating on rock damage could not be assessed. However, another in-situ heating test, SE-H, was subsequently performed as part of the TIMODAZ project (Li et al. 2011). Heating was applied by circulating water at a high temperature through a packer-isolated section of a 76mm diameter borehole installed in the shaly facies of Opalinus Clay. A number of hydraulic tests were performed in an adjacent borehole interval. It was found that after a temperature increase to about 65ºC, intrinsic permeability reduced by a factor of 4. So no adverse effects in terms of rock damage appear to result from an increase of temperature, rather the opposite.

6. Concluding remarks

The understanding of the behaviour of Opalinus Clay under thermal loading has been much advanced by the performance and study of a number of in-situ heating tests: HE-B, HE-D and HE-E. Those tests cover a wide range of test layouts and conditions. In spite of this, the observed behaviour of Opalinus clay is quite similar in the three cases. Although the temperatures applied by the heaters are rather high, the temperature increases in the Opalinus Clay have been generally moderate because of the rapid thermal attenuation with distance and of the isolating nature of the engineered barriers in tests HE-B and HE-E. In spite of those modest increases, the generation of pore pressures has been very significant in all cases. The mechanism underlying the generation of pore pressures is well understood; it arises from the combination of the effects of differential rock/water thermal dilation and of pore pressure dissipation, controlled by rock permeability. There is less information on thermal effects on mechanical variables; strains measured in the HE-D test, however, turn out to be quite small. Hydraulic measurements carried out in a different test, SE-H, suggest that heating might be beneficial with respect to rock damage as the intrinsic permeability reduced significantly after an increase of temperature.

The HE-D test has been analysed in more detail because it involves no engineered barrier, so the behaviour of Opalinus Clay under thermal loading can be examined more directly. From those analyses, it is possible to assess the various THM phenomena involved and evaluate their relative importance (Gens 2010):

- the strongest coupling corresponds to the effects of the thermal field on hydraulic and mechanical behaviour. Pore pressure increases are caused by temperature rises

whereas thermal expansion is the most important source of rock deformation and displacements. Deformations and displacements are however small.

- noticeable but more modest effects result from the coupling of hydraulic phenomena to mechanical behaviour. The dissipation of pore pressures induces additional displacements and strains that, due to the high Opalinus Clay stiffness, are smaller than thermally-induced deformations.
- in principle, mechanical damage could impact the hydraulic observations if a zone of higher permeability develops due to material damage. However no such thermally-induced damaged zone has been observed; in fact a reduction of permeability has been observed in the rock affected by temperature increase
- there is no perceptible coupling from hydraulic and mechanical phenomena to thermal behaviour. Practically all heat transport is by conduction and the thermal conductivity of the material does not change as deformations are small the material remains saturated throughout. In addition, mechanical energy dissipation is negligible in a non-isothermal case.

Acknowledgements

The authors are grateful to the reviewers of the Paper, Prof. Pierre Delage, Ecole des Ponts ParisTech, Laboratoire Navier, CERMES, France and Dr. Xiangling Li, Belgian Nuclear Research Centre, Mol, Belgium for their comments and suggestions.

References

Auvray, C. (2004). Thermomechanical tests on Opalinus Clay of the Mont Terri, *ANDRA internal report, C.RP.OENG.04-0239.* Agence Nationale pour la Gestion des Déchets Radioactifs (ANDRA), Bure, France. www.andra.fr

Booker, J. R., & Savvidou, C. (1985). Consolidation around a point heat source. *International Journal for Numerical and Analytical Methods in Geomechanics, 9,* 173-184.

Bossart, P. (2008). Annex 4. Characteristics of the Opalinus clay at Mont Terri. In P. Bossart, & M. Thury (Eds.), *Mont Terri Rock Laboratory. Project, Programme 1996 to 2007 and Results. Reports of the Swiss Geological Survey, No. 3* (445 pp). Federal Office of Topography (swisstopo), Wabern, Switzerland. www.mont-terri.ch

Carslaw H. S., & Jaeger J. C. (1946). *Conduction of heat in solids* (520 pp.). London: Oxford University Press

Garitte, B., Gens, A., Vaunat, J., & Armand, G. (2014). Thermal conductivity of argillaceous rocks: Determination methodology using in situ heating tests. *Rock Mechanics Rock Engineering, 47*, 111-129.

Gaus, I., Garitte, B., Senger, R., Gens, A., Vasconcelos, R., Garcia-Sineriz, J. L & Mayor, J. C. (2014). The HE-E experiment: Lay out, Interpretation and THM modelling. *Nagra Arbeitsbericht NAB 14-53,* 178 pp. Nagra, Wettingen, Switzerland. www.nagra.ch

Gens, A. (2010). Soil-environment interactions in geotechnical engineering. *Géotechnique, 60,* 3-74.

Gens, A., Vaunat, J., Garitte, B., & Wileveau, Y. (2007). In situ behaviour of a stiff layered clay subject to thermal loading: observations and interpretation. *Geotechnique, 57,* 207-228.

Göbel, I., Alheid, H.-J., Alonso, E., Ammon, C., Bossart, P., Brühler, C., Emmerich, K., Fernandez, A. M., García-Siñeriz, J. L., Graf, A., Jockwer, N., Kaufhold, S., Kech, M., Klubertanz, G., Lloret, A., Mayor, J. C., Meyer, T., Miehe, R., Muñoz, J. J., Naumann, M., Nussbaum, C., Pletsch, T., Plischke, I., Ploetze, M., Rey, M., Schnier, H., Schuster, K., Sprado, K., Trick, T., Weber, H., Wieczoreck, K., & Zingg, A. (2007). Heater Experiment: Rock and bentonite thermo-hydro-mechanical (THM) processes in the near field of a thermal source for development of deep underground high level radioactive waste repositories. In P. Bossart, & C. Nussbaum (Eds.), *Mont Terri Project - Heater Experiment,, Engineered Barriers Emplacement and Ventilation Tests*. Report of the Swiss Geological Survey No. 1 (pp. 7-16). Federal Office of Topography (swisstopo), Wabern, Switzerland. www.mont-terri.ch

Li, X.-L., Arson, C., Bastiaens, W., Bernier, F., Blaser, P., Bésuelle, P., Charlier, R., Chambon, R., Collin, F., Czímerová, A., Delage, P., Dedecker, F., Dizier, A., De Craen, M., Fauriel, S., François, B., Fisch, H., Fierz, T., Fokkens, J., Garitte, B., Gens, A., Gatmiri, B., Gérard, P., Guangjing, C., Gastaldo, L., Honty, M., Reyes-Montes, J.M., Haycox, J. H., Jaap, H., Andrews, J.R., Vincent, L., Laloui, L., Levorova, M., Lebon, P., Li, X. L., Li, Y., Illing, P.,

Levasseur, S., Monfared, M., Marinelli, F., Meynet, T., Madejová, J., Osacký, M., Pacovsky, J., Radu, J.-P., Rizzi, M., Sieffert, Y., Sillen, X., Sauthier, C., Salager, S., Schroeder, C., Sulem, J., Viggiani, G., Van Marcke, P., Vaunat, J., Vietor, T., Verstricht, J., Vasicek, R., Vigne, L., Wang, L., Weetjens, E.,Pettitt, W.S., You, S., & Zhang, Z. (2001). *TIMODAZ. Thermal Impact on the Damage Zone Round a Radioactive Waste Disposal in Clay Host rocks. Final Activity Report. Contract Number FI6W-CT-2007-036449* (60 pp.). European Commission, Brussel, Belgium.

Vaunat, J., & Gens, A. (2003a). Bond degradation and irreversible strains in soft argillaceous rock. In *Proceedings of the 12th Panamerican conference on soil mechanics and geotechnical engineering*, Boston, 1, 479-484.

Vaunat, J., & Gens, A. (2003b). Numerical modelling of an excavation in a hard soil/soft rock formation using a coupled damage/plasticity model. In *Proceedings of the VII International Conference on Computational Plasticity*, COMPLAS (Oñate and Owen, eds.), Barcelona: CIMNE.

Wileveau, Y. (2005). THM behaviour of host rock (HE-D) experiment: Progress Report. Part 1. *Mont Terri Technical Report,* TR 05-03, 129 pp. Mont Terri Project. Federal Office of Topography (swisstopo), Wabern, Switzerland. www.mont-terri.ch

Wileveau, Y., Göbel, I., Huertas, F., Jockwer, N., Schnier, H., Schnier, H., Shimura, T., Weber H. P., Yamamoto, S., & Zhang, C.-L. (2008). Thermal properties and THMC experiments. In Bossart, P. and Thury, M. (Eds.), *Mont Terri Rock Laboratory. Project,*

Programme 1996 to 2007 and Results. Report of the Swiss Geological Survey No. 3 (pp. 145-153). Federal Office of Topography (swisstopo), Wabern, Switzerland. www.mont-terri.ch

Figure captions

Figure 1. Geological profile of the Mont Terri rock laboratory site

Figure 2. Coupled Thermo-hydro-mechanical (THM) phenomena

Figure 3. Location of the main heating tests performed in the Mont Terri rock laboratory

Figure 4.Central borehole layout and location of the central and instrumentation boreholes in the niche. Experiment HE-B.

Figure 5. Distributions of Opalinus Clay temperatures at various times during the heating period. Experiment HE-B.

Figure 6. Thermal-induced pore pressures in Opalinus Clay measured in boreholes BHE-19 and BHE-20 (see Figure3). Experiment HE-B.

Figure 7. Schematic layout of the in-situ test HE-D. Locations of observations boreholes are shown.

Figure 8. Evolution of temperature at different distances of the heater axis. Experiment HE-D.

Figure 9. Evolution of thermally-induced pore pressures at different distances of the heater axis. Experiment HE-D.

Figure 10. Schematic layout of the HE-E experiment

Figure 11. Evolution of the heater power in HE-E experiment

Figure 12. Evolution of temperatures in Opalinus Clay in the vicinity of Heater 1. HE-E experiment

Figure 13. Evolution of thermally-induced pore pressures in Opalinus Clay. HE-E experiment

Figure 14. Thermal conductivity pairs that result in an error of less than 2% computed at different times since the start of heating. Figure 13. Thermal conductivity pairs that result in an error of less than 2% computed at different times since the start of heating. Point heat source case.

Figure 15. Best fitting thermal conductivity pairs for different sensors in the HE-D test. The stars indicate the average thermal conductivity values for two different hypotheses of heating power. The parameter α in the Figure indicates anisotropy ratio; the curves corresponding to constant values of equivalent thermal conductivity, λ_0, are also shown.

Figure 16. Evolution of temperature and pore pressure in borehole D3 during the HE-D test.

Figure 17. Evolution of pore pressure increments at various points in the Opalinus Clay during the HE-D test. Observations and computed results a) Borehole D03, b) Borehole D14, c) Borehole D15, d) Borehole D16, e) Borehole D17, f) Sensor location

Figure 18. Computed pore pressure increment distributions at various times on a section across Heater 2 in the HE-D test. a) Bedding plane direction b) Perpendicular to bedding plane direction

Figure 19. Computed contours of pore pressure increase in the HE-D test. a) 90 days (end of 1st heating stage), b) 93 days, c) 110 days (pore pressure maxima), d) 297 days, e) 346 days (start of cooling phase), f) 509 days (end of test).

Figure 20. Effect on intrinsic permeability on pore pressure evolution. a) Permeability parameters in the range of realistic values. b) Undrained and drained conditions.

Figure 21. Distributions of deformation measured at different times in borehole D5, drilled approximately perpendicular to the main borehole. HE-D test.

Figure 22. Evolution of strain increments at various points in the Oplinus clay (Borehole D5). Observed and computed results. HE-D test.

Table caption

Table 1. Features of the main in-situ heating tests performed in the Mont Terri rock laboratory

Figures

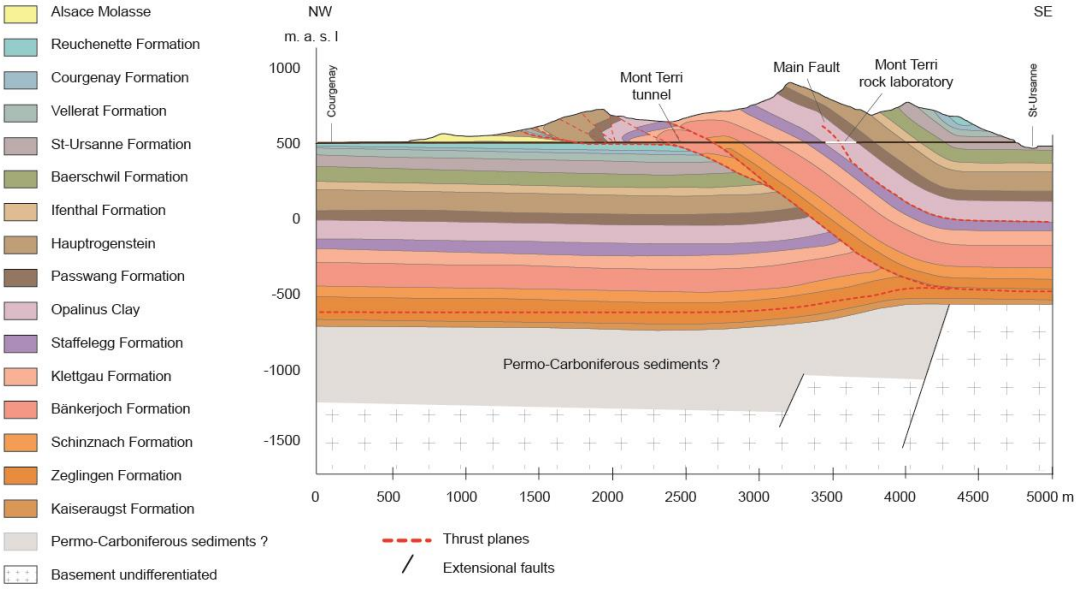

Figure 1. Geological profile of the Mont Terri rock laboratory site

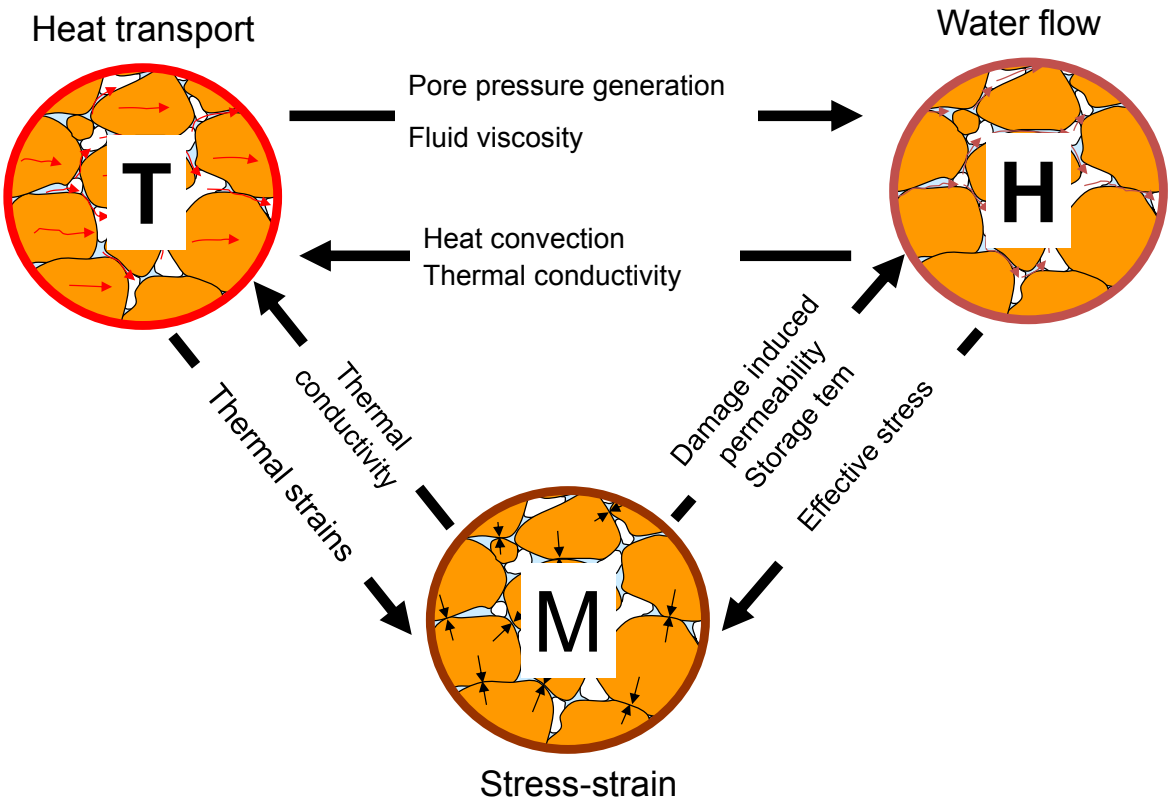

Figure 2. Coupled Thermo-hydro-mechanical (THM) phenomena

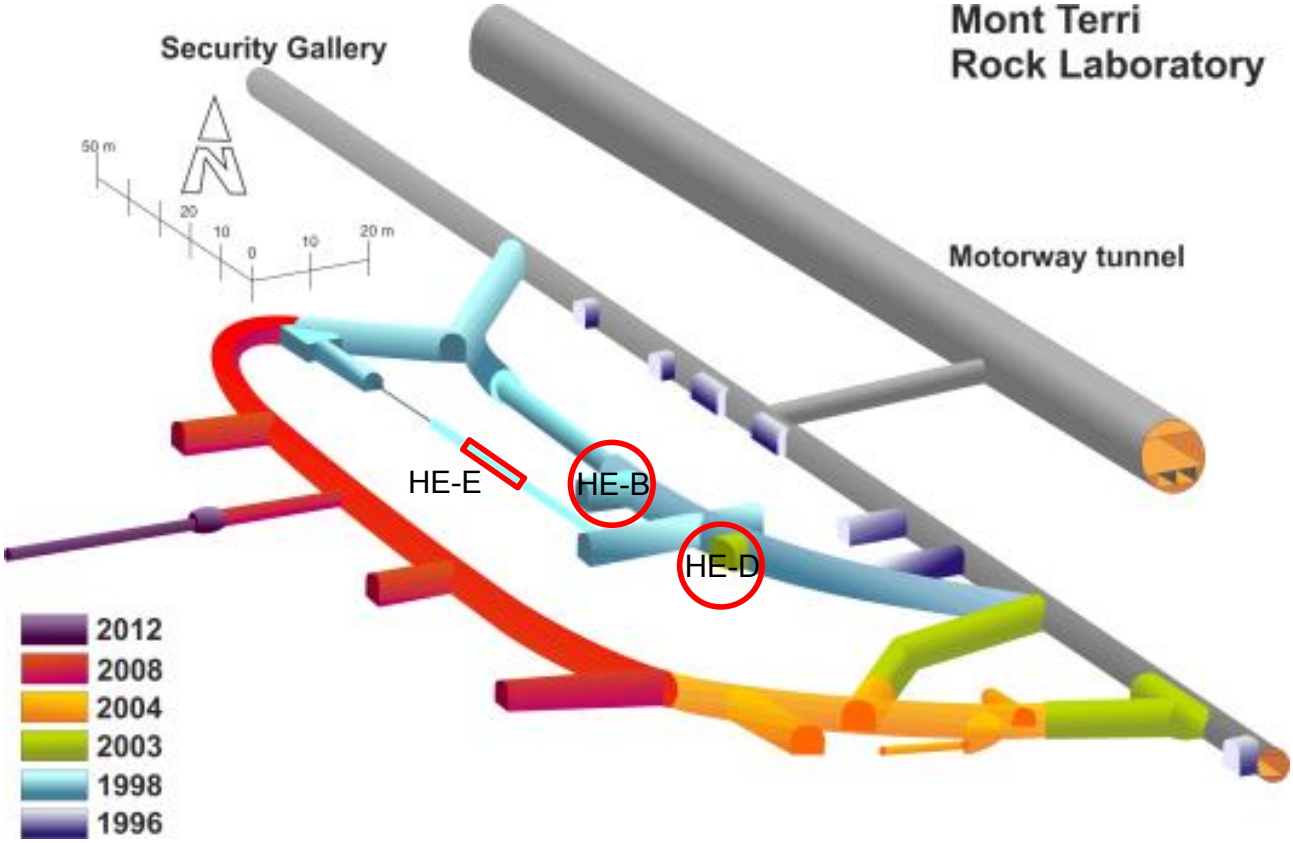

Figure 3. Location of the main heating tests performed in the Mont Terri rock laboratory

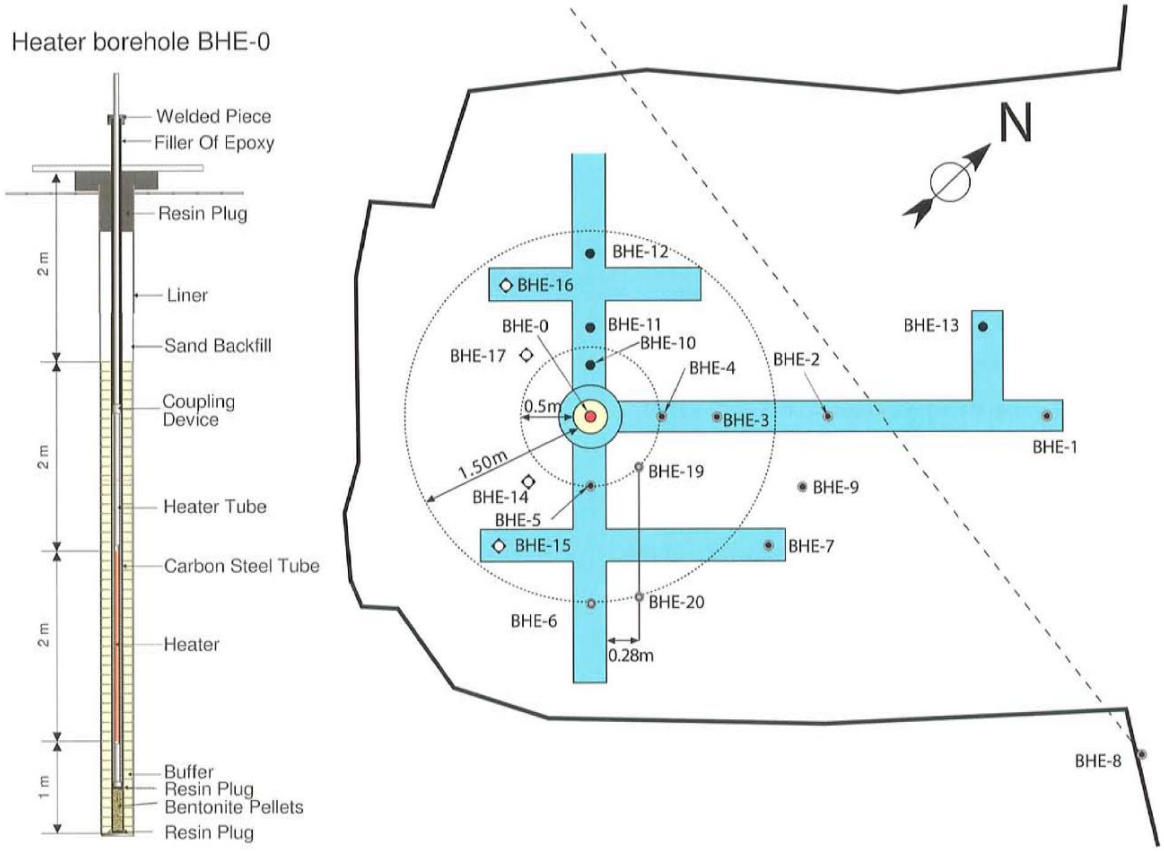

Figure 4.Central borehole layout and location of the central and instrumentation boreholes in the niche. Experiment HE-B.

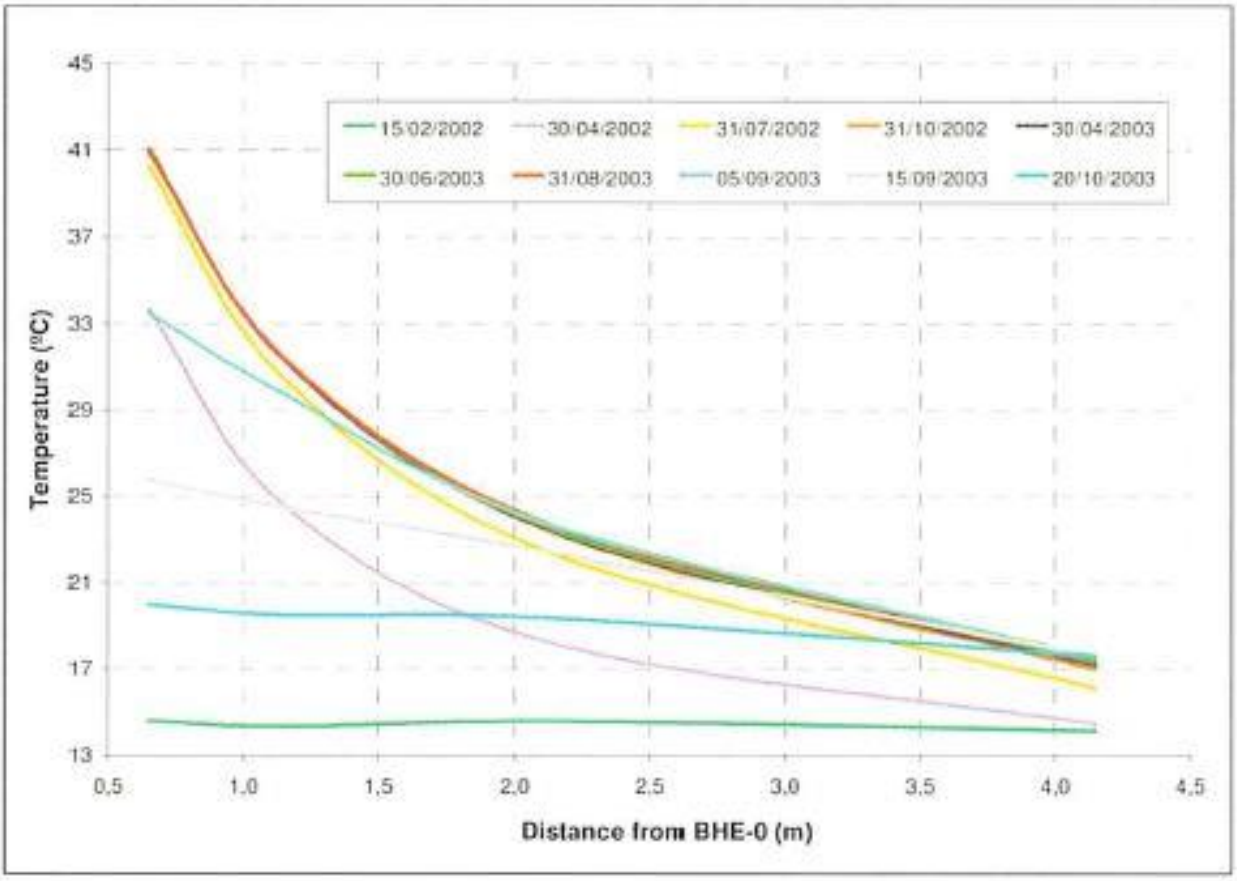

Figure 5. Distributions of Opalinus Clay temperatures at various times during the heating period. Experiment HE-B.

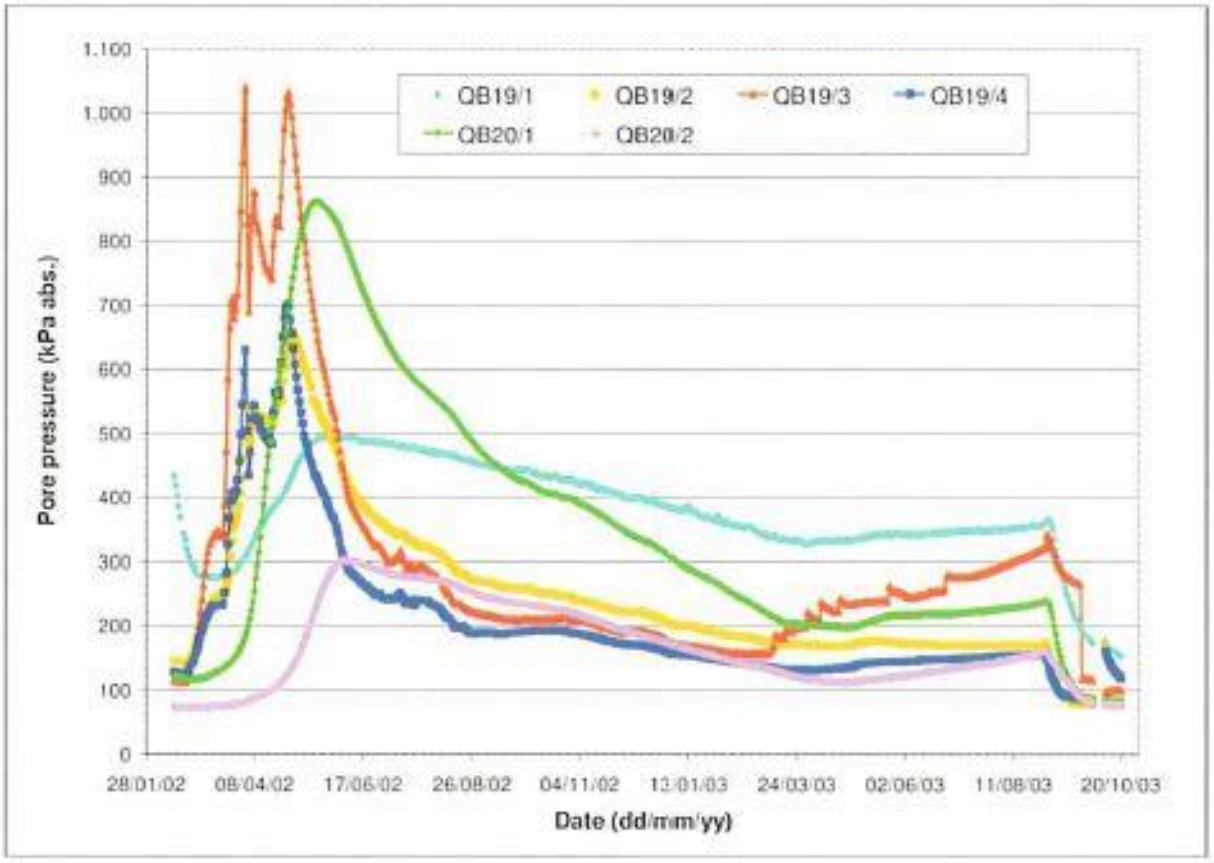

Figure 6. Thermal-induced pore pressures in Opalinus Clay measured in boreholes BHE-19 and BHE-20 (see Figure3). Experiment HE-B.

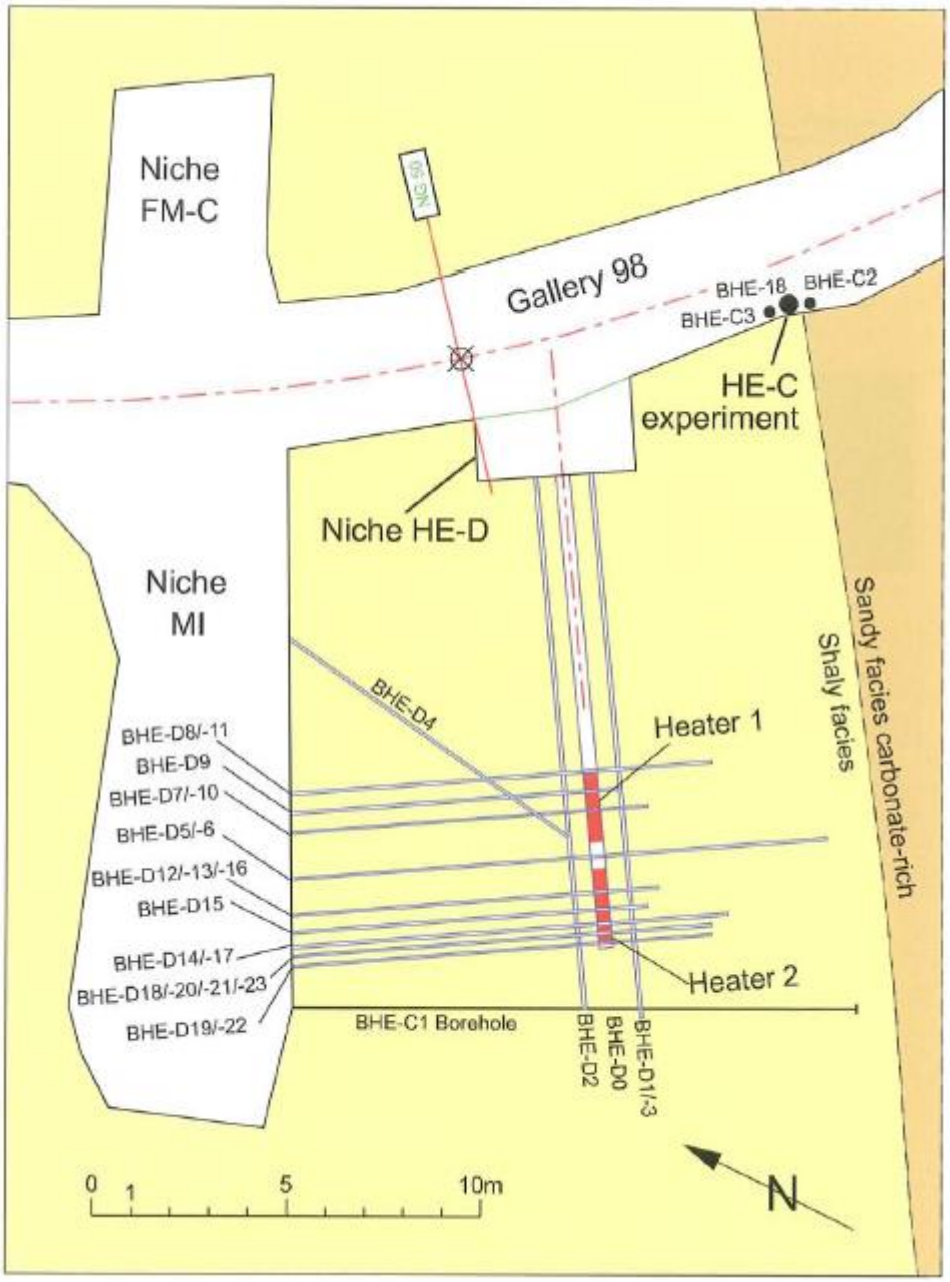

Figure 7. Schematic layout of the in-situ test HE-D. Locations of observations boreholes are shown.

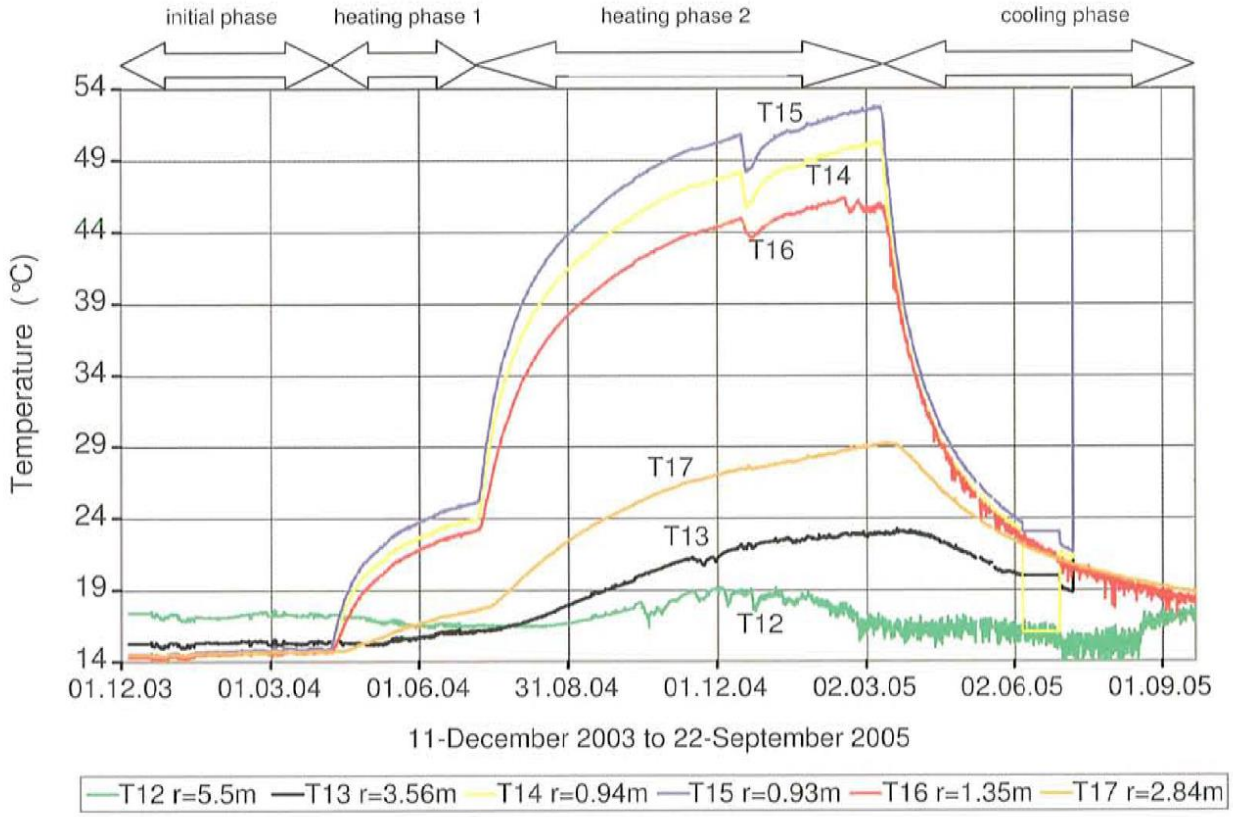

Figure 8. Evolution of temperature at different distances of the heater axis. Experiment HE-D.

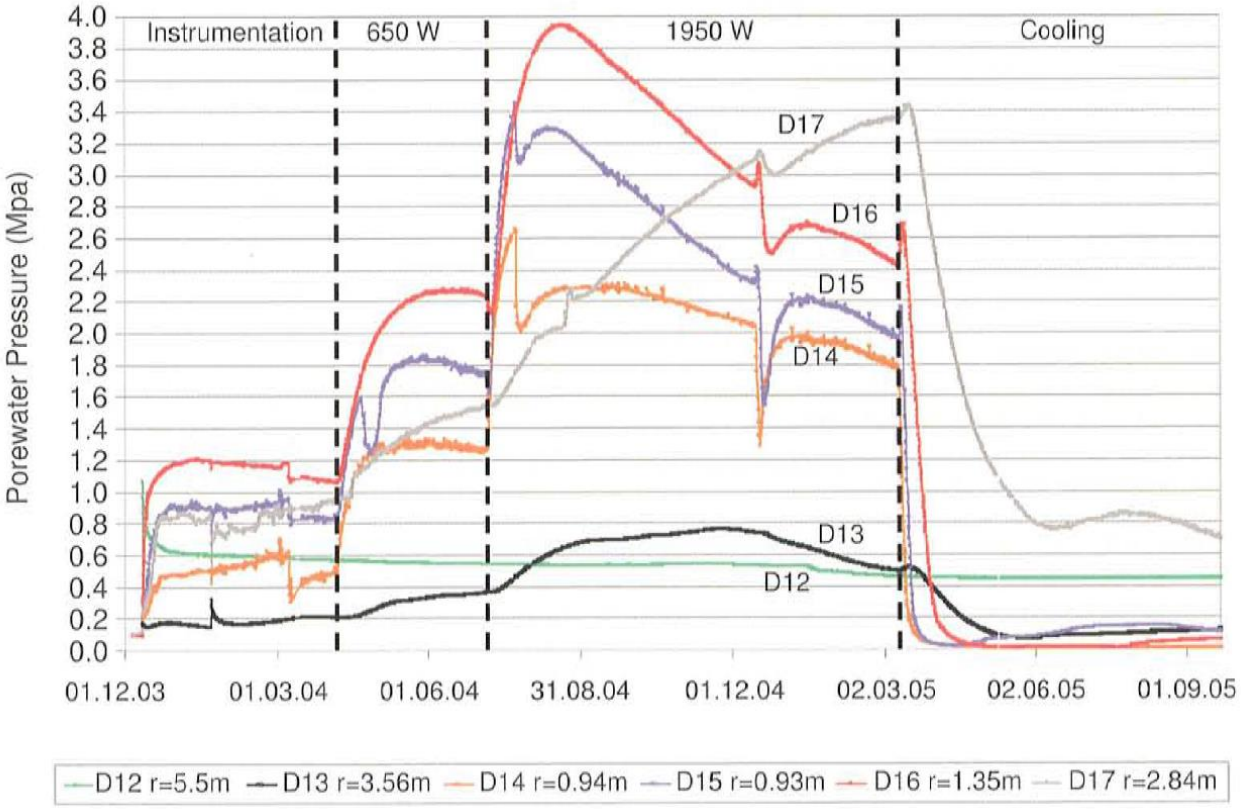

Figure 9. Evolution of thermally-induced pore pressures at different distances of the heater axis. Experiment HE-D.

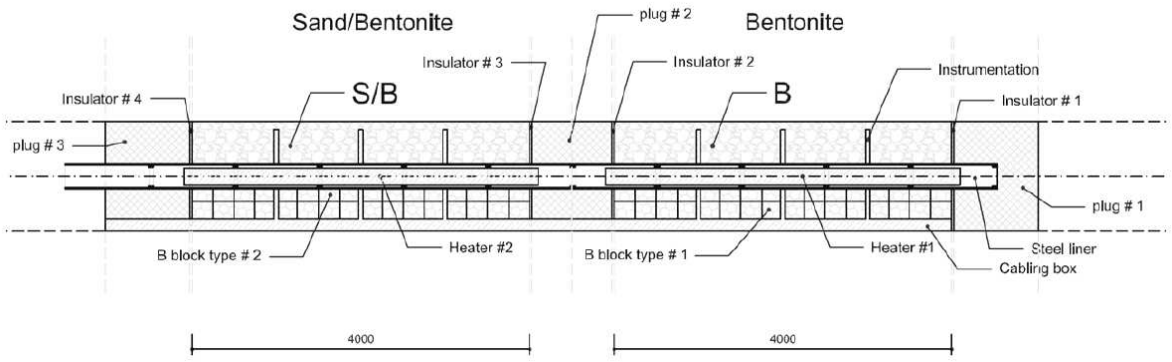

Figure 10. Schematic layout of the HE-E experiment

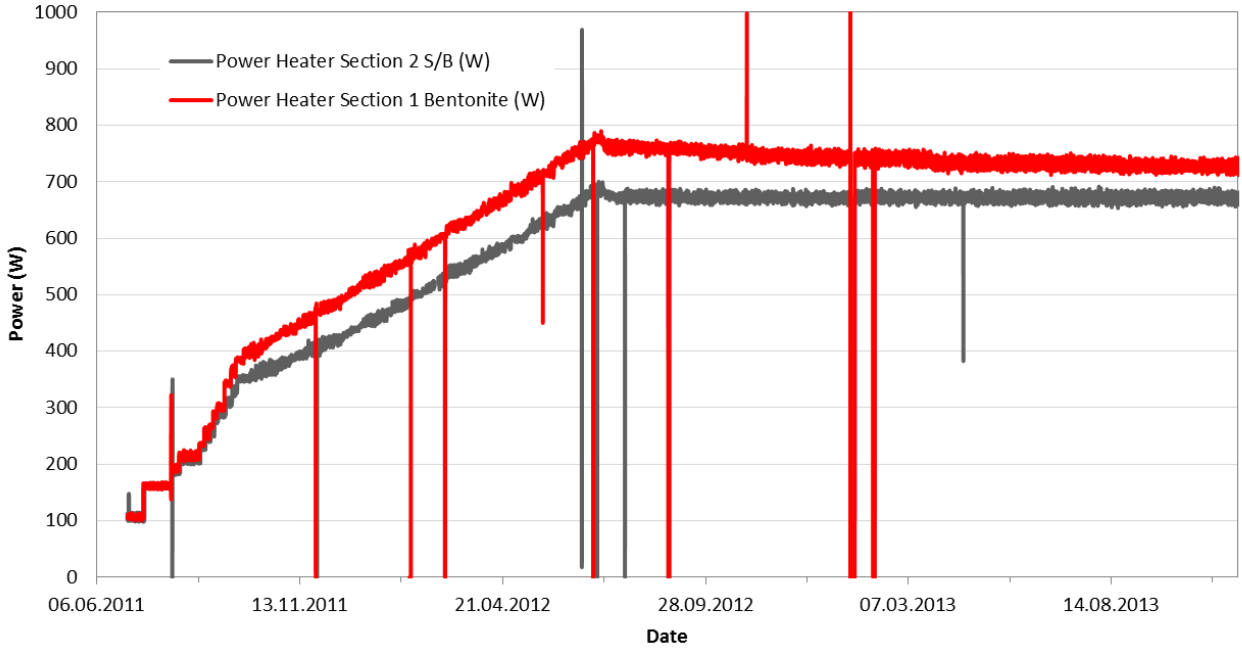

Figure 11. Evolution of the heater power in HE-E experiment

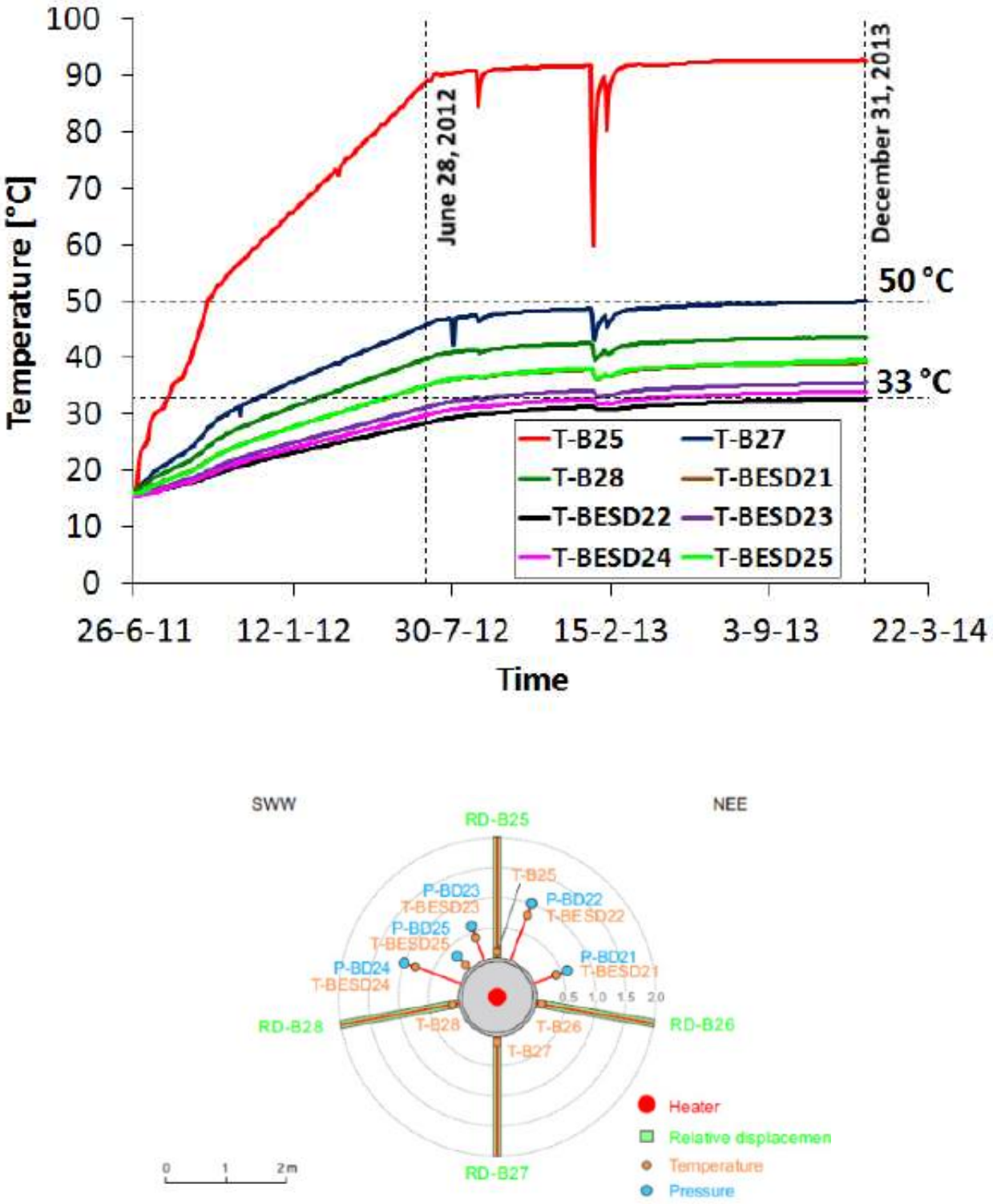

Figure 12. Evolution of temperatures in Opalinus Clay in the vicinity of Heater 1. HE-E experiment

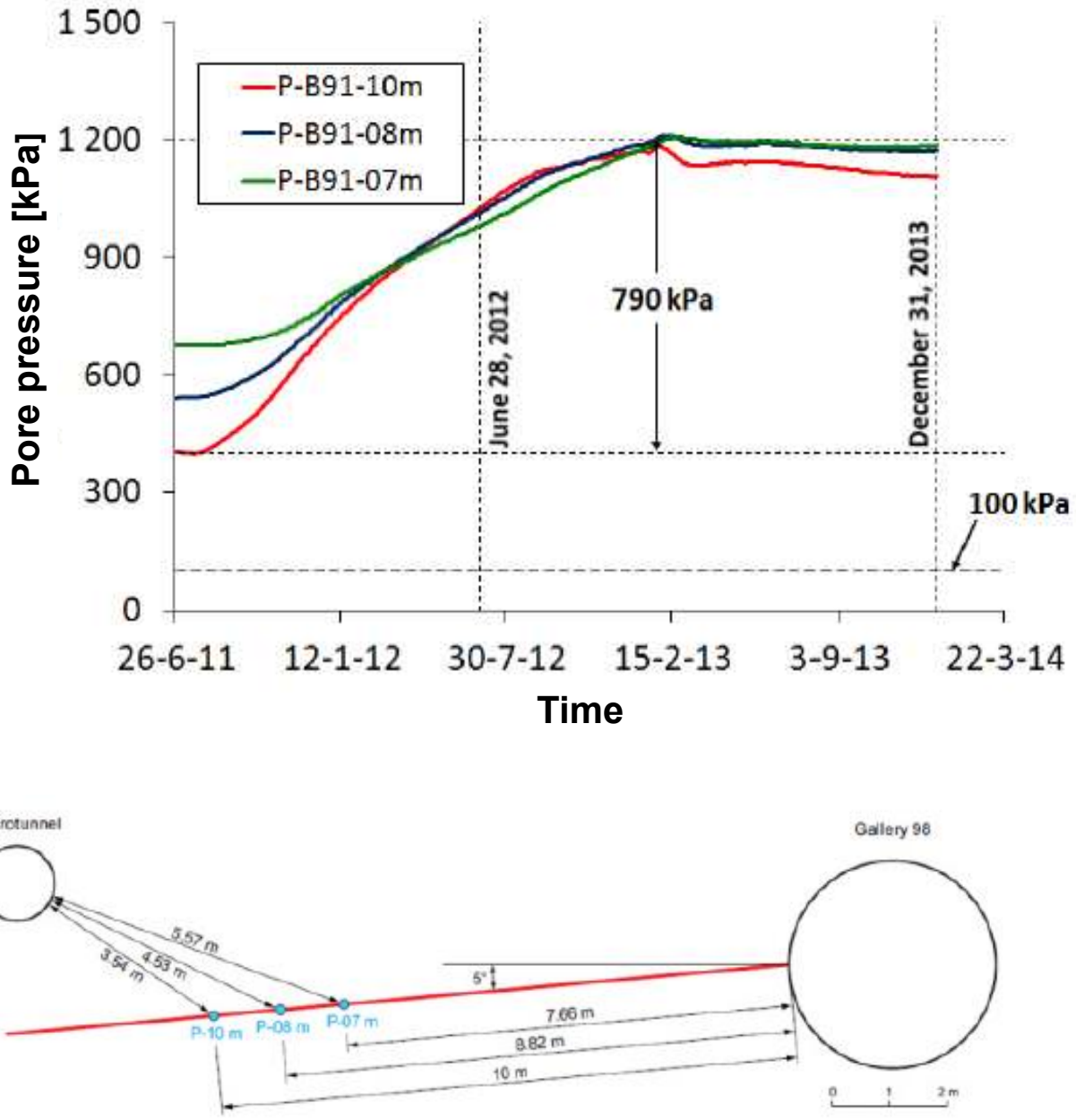

Figure 13. Evolution of thermally-induced pore pressures in Opalinus Clay. HE-E experiment

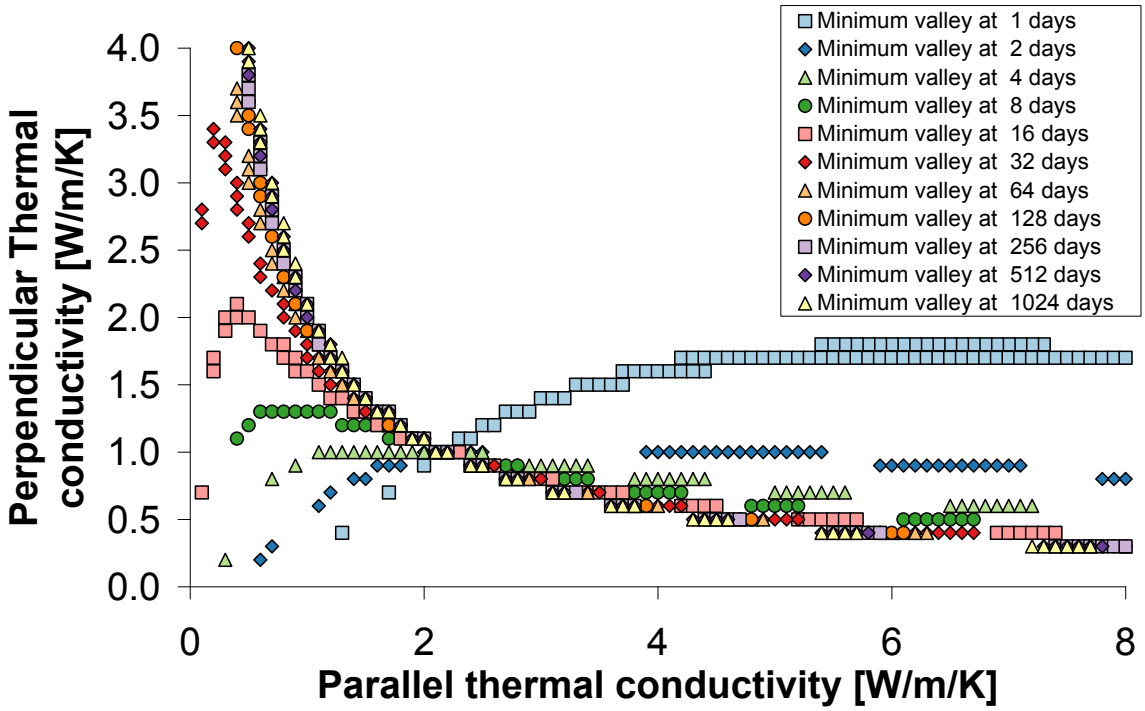

Figure 14. Thermal conductivity pairs that result in an error of less than 2% computed at different times since the start of heating. Point heat source case.

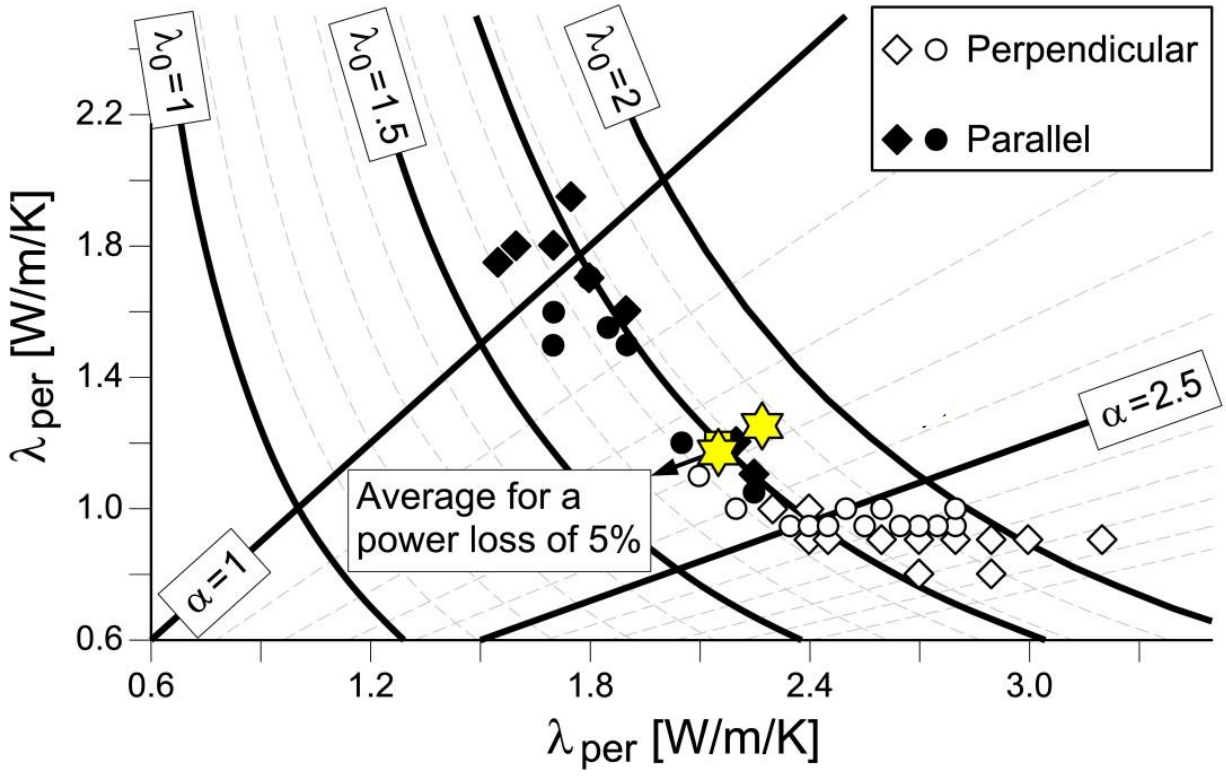

Figure 15. Best fitting thermal conductivity pairs for different sensors in the HE-D test. The stars indicate the average thermal conductivity values for two different hypotheses of heating power. The parameter α in the Figure indicates anisotropy ratio; the curves corresponding to constant values of equivalent thermal conductivity, λ_0, are also shown.

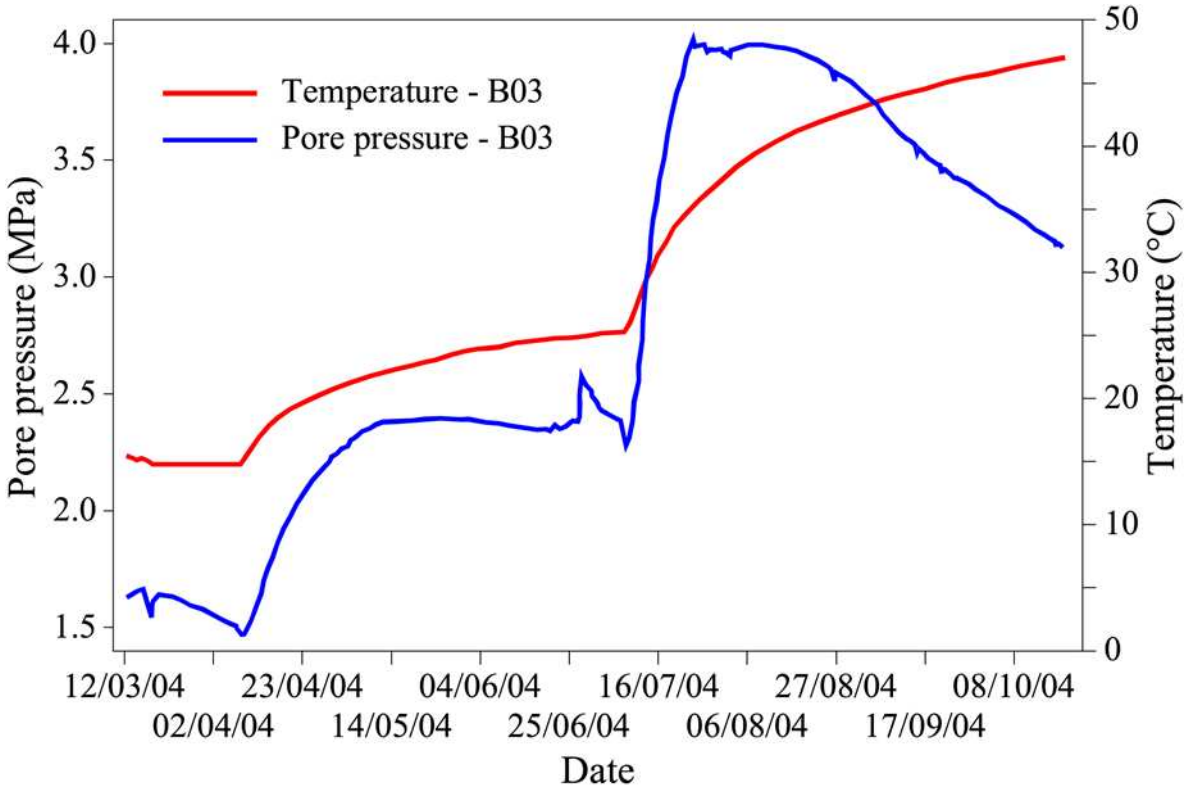

Figure 16. Evolution of temperature and pore pressure in borehole D3 during the HE-D test.

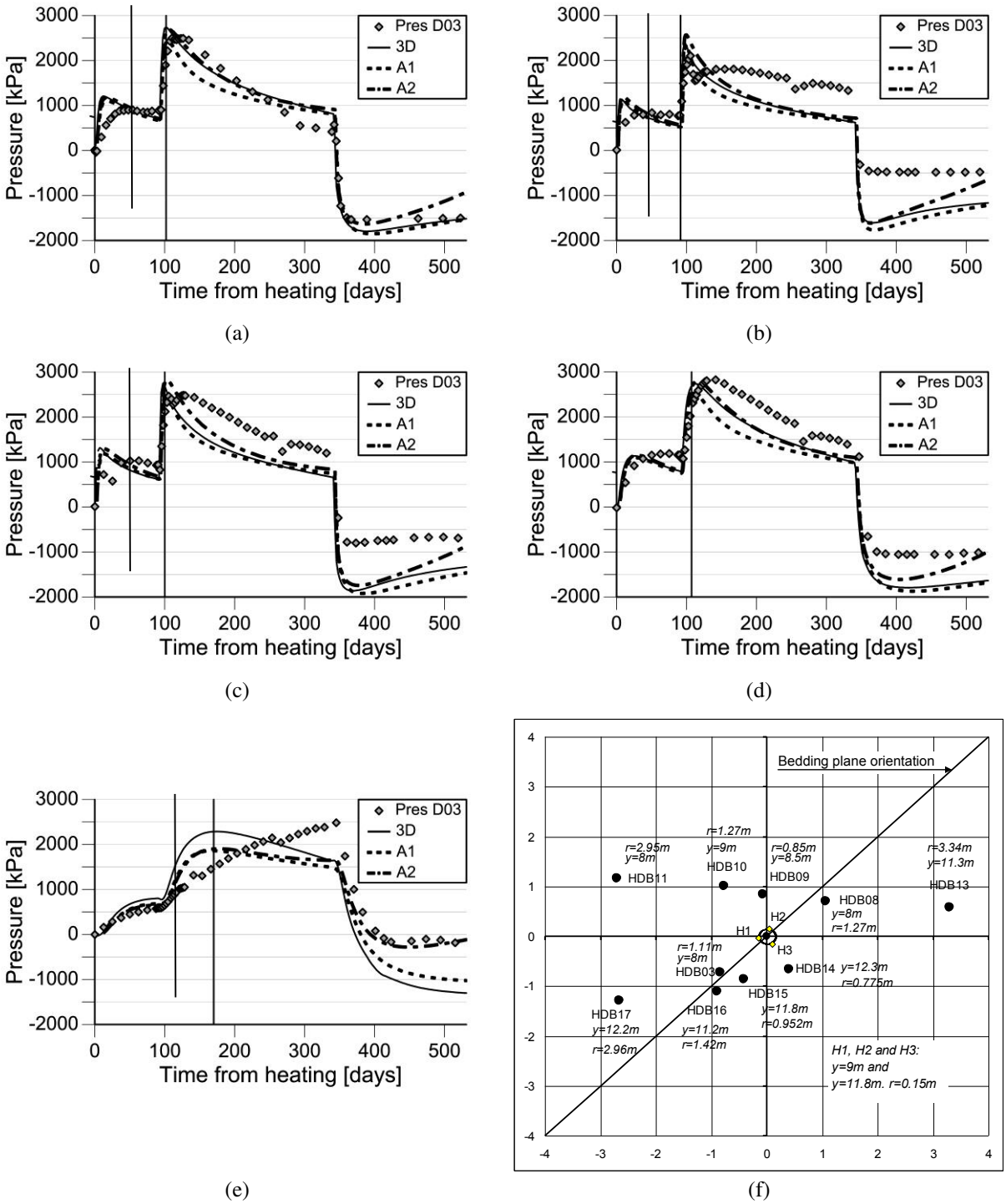

Figure 17. Evolution of pore pressure increments at various points in the Opalinus Clay during the HE-D test. Observations and computed results a) Borehole D03, b) Borehole D14, c) Borehole D15, d) Borehole D16, e) Borehole D17, f) Sensor location

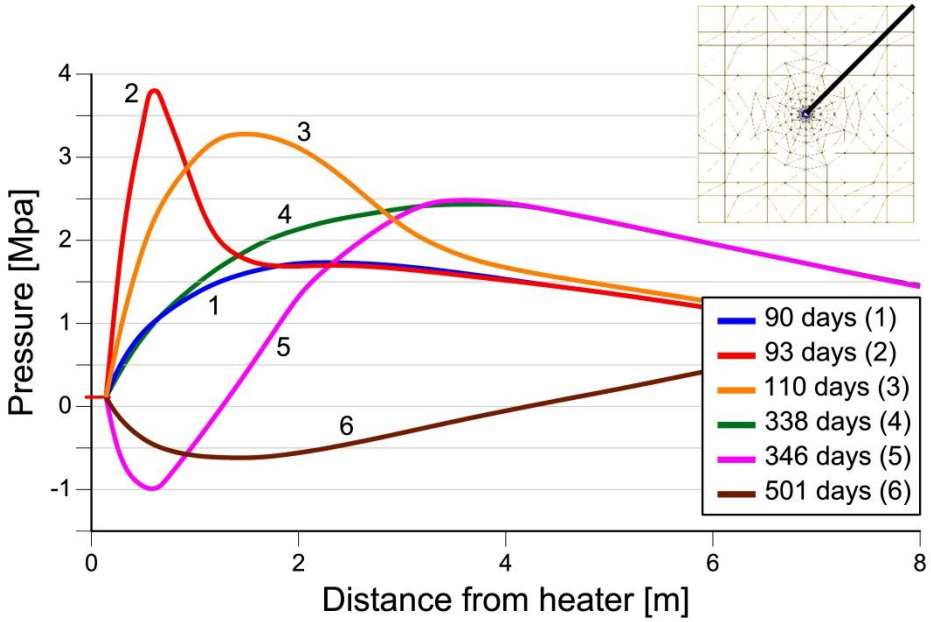

(a)

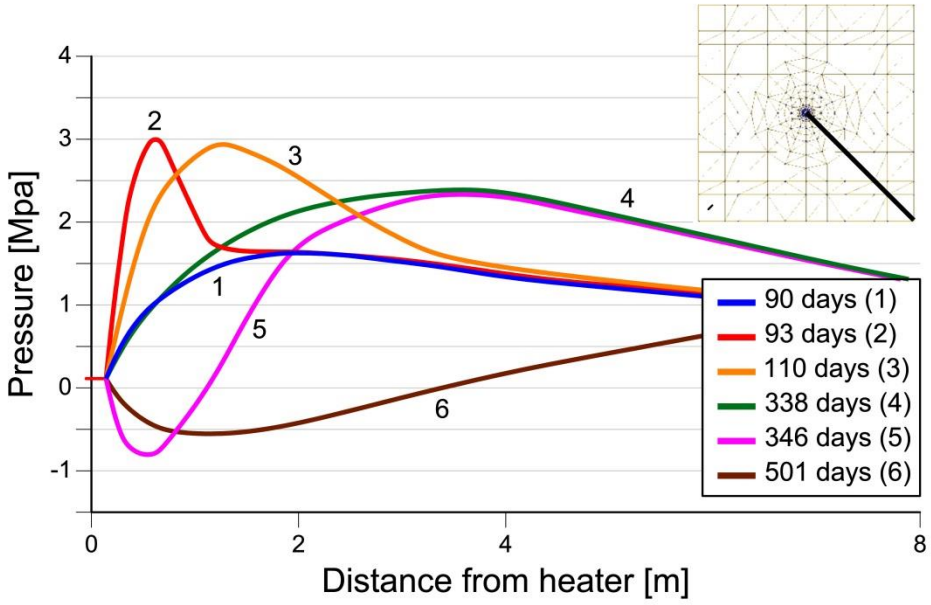

(b)

Figure 18. Computed pore pressure increment distributions at various times on a section across Heater 2 in the HE-D test. a) Bedding plane direction b) Perpendicular to bedding plane direction

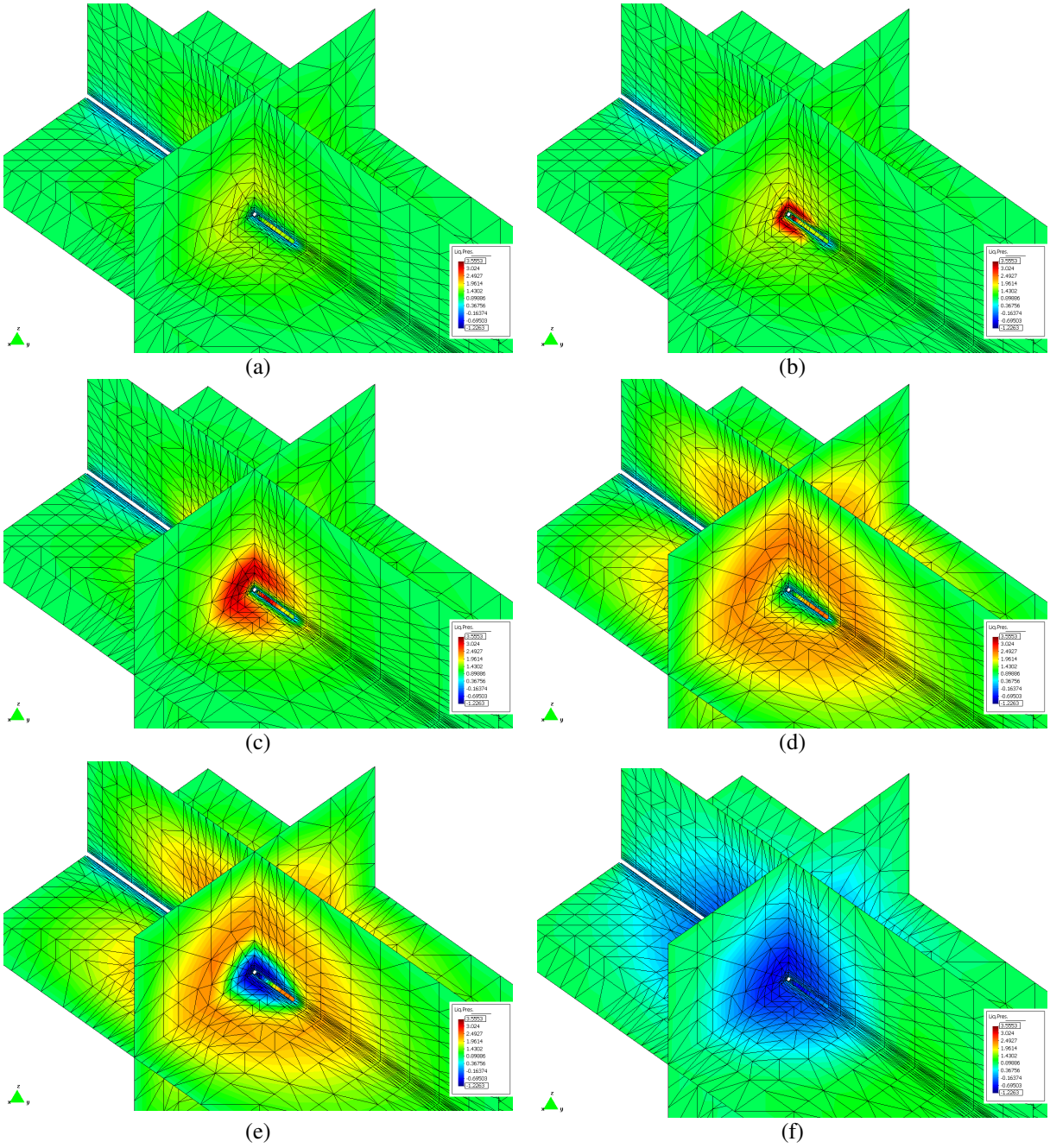

Figure 19. Computed contours of pore pressure increase in the HE-D test. a) 90 days (end of 1st heating stage), b) 93 days, c) 110 days (pore pressure maxima), d) 297 days, e) 346 days (start of cooling phase), f) 509 days (end of test).

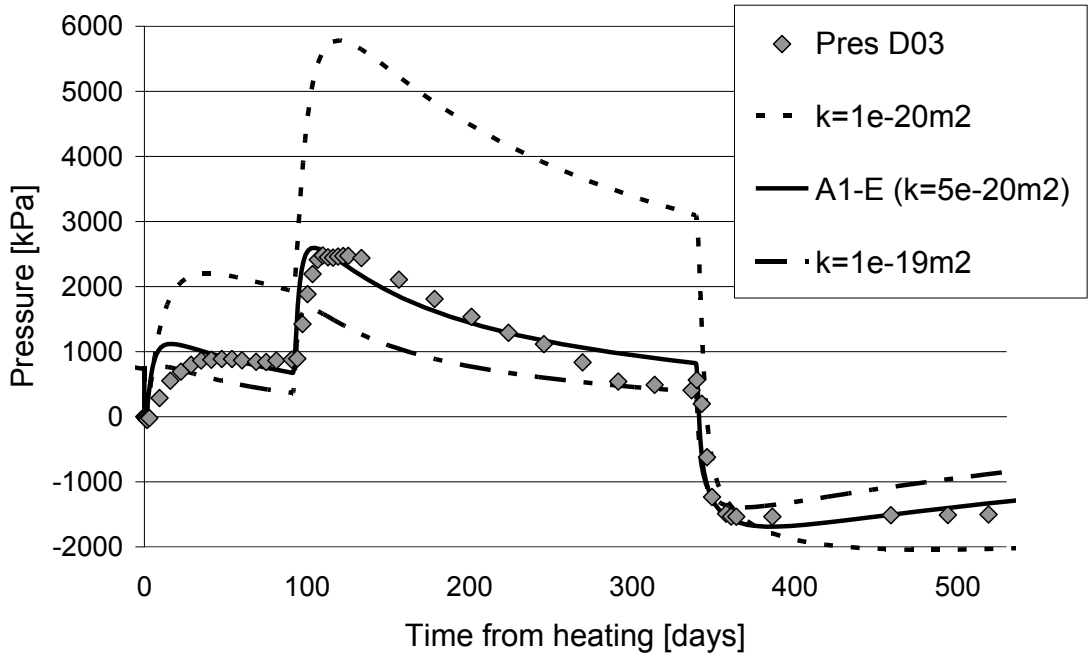

a)

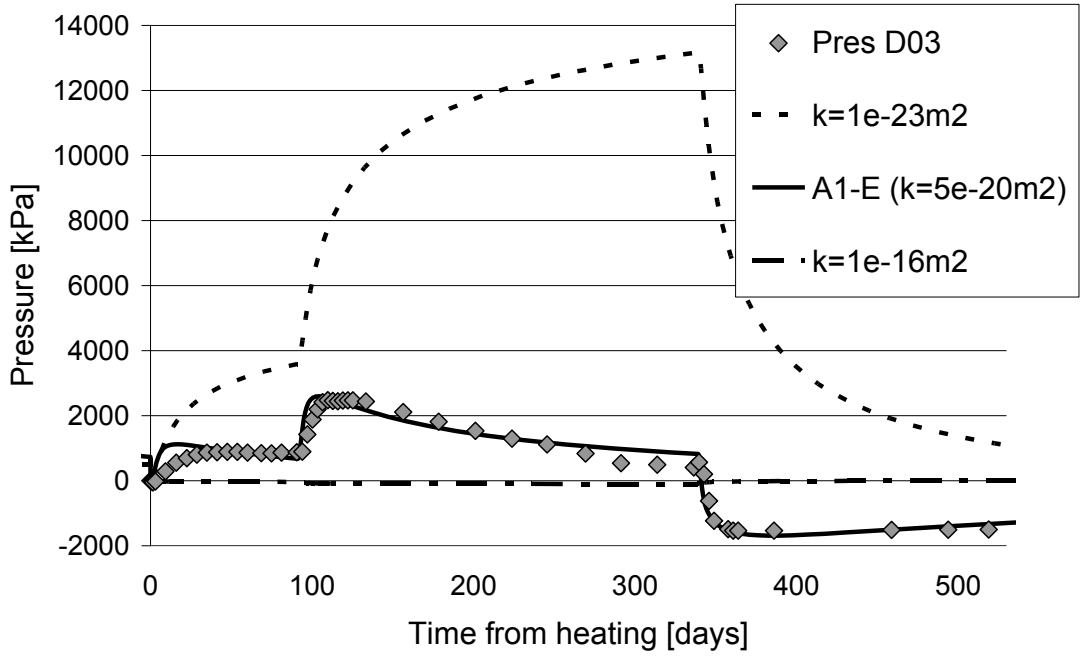

b)

Figure 20. Effect on intrinsic permeability on pore pressure evolution. a) Permeability parameters in the range of realistic values. b) Undrained and drained conditions

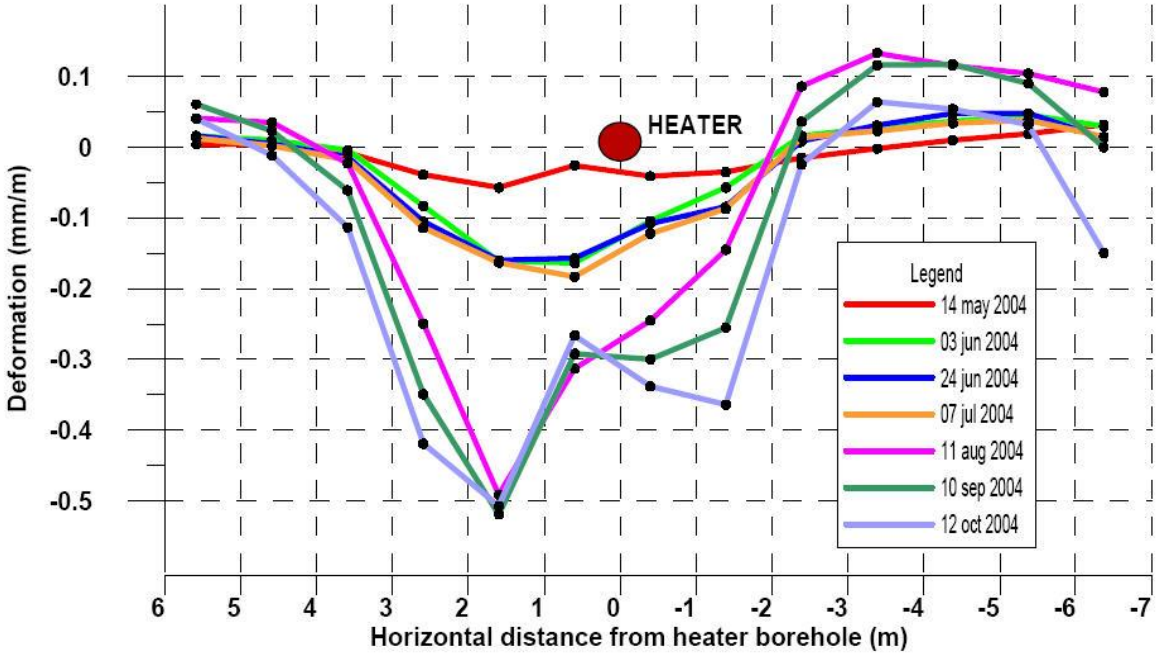

Figure 21. Distributions of deformation measured at different times in borehole D5, drilled approximately perpendicular to the main borehole. HE-D test.

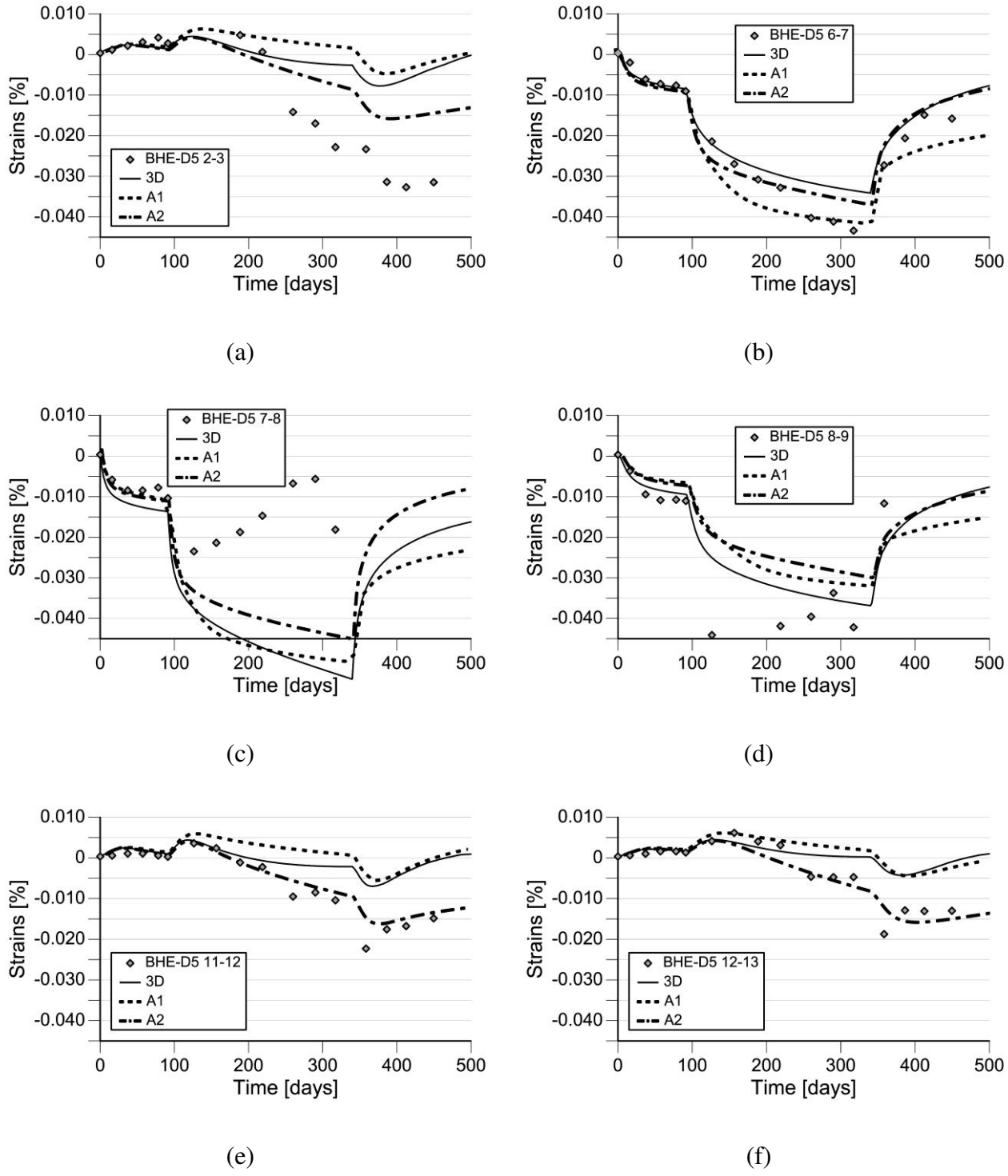

Figure 22. Evolution of strain increments at various points in the Oplinus clay (Borehole D5). Observed and computed results. HE-D test.

Table

Experiment	HE-B (HE)	HE-D	HE-E
Borehole /Tunnel	Vertical	Horizontal	Horizontal
Borehole /Tunnel diameter	0.3 m	0.3 m	1.3 m
Heater/liner diameter	0.1 m	0.3 m	0.3 m
Heater length	2.02 m	2 x 2 m	2 x 4 m
Max. heater temperature	100ºC	100ºC	140ºC
Backfill thickness	0.1 m	-	0.5 m
Backfill material	Compacted blocks (Febex bentonite)	-	Granular bentonite (MX80, MX80+sand)
Backfill hydration	Artificial	-	Natural
Heating duration	18 months	11 months	Long term
Heating period	February 2002 – August 2003	March 2004 – February 2005	June 2011 - ?

Table 1. Features of the main in-situ heating tests performed in the Mont Terri rock laboratory